AD-A086 869 PENNSYLVANIA UNIV PHILADELPHIA F/G 11/9
CONDUCTING ORGANIC POLYMERS: DOPED POLYACETYLENE,(U)
NOV 79 A J HEEGER, A G MACDIARMID N00014-75-C-0962
UNCLASSIFIED TR-79-10 NL

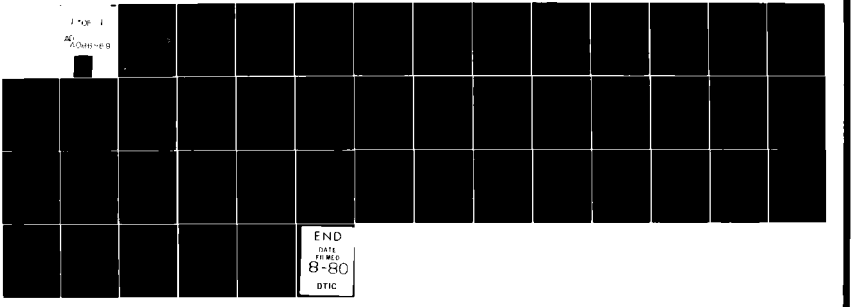

Unclassified

SECURITY CLASSIFICATION OF THIS PAGE (When Data Entered)

REPORT DOCUMENTATION PAGE

READ INSTRUCTIONS BEFORE COMPLETING FORM

1. REPORT NUMBER	2. GOVT ACCESSION NO.	3. RECIPIENT'S CATALOG NUMBER
Technical Report No. 79-10	AD-A086 869	

4. TITLE (and Subtitle)

Conducting Organic Polymers: Doped Polyacetylene

5. TYPE OF REPORT & PERIOD COVERED

Interim Technical Report

6. PERFORMING ORG. REPORT NUMBER

7. AUTHOR(s)

A.J. Heeger[+] and A.G. MacDiarmid[≠]

8. CONTRACT OR GRANT NUMBER(s)

N00014-75-C-0962

9. PERFORMING ORGANIZATION NAME AND ADDRESS

Department of Physics[+] and Department of Chemistry[≠]
University of Pennsylvania, Laboratory for Research on the Structure of Matter, Phila., Pa. 19104

10. PROGRAM ELEMENT, PROJECT, TASK AREA & WORK UNIT NUMBERS

NR-356-602

11. CONTROLLING OFFICE NAME AND ADDRESS

Department of the Navy
Office of Naval Research
Arlington, Va. 22217

12. REPORT DATE

November 24, 1979

13. NUMBER OF PAGES

40

14. MONITORING AGENCY NAME & ADDRESS (if different from Controlling Office)

15. SECURITY CLASS. (of this report)

unclassified

15a. DECLASSIFICATION/DOWNGRADING SCHEDULE

16. DISTRIBUTION STATEMENT (of this Report)

Distribution unlimited; approved for public release

17. DISTRIBUTION STATEMENT (of the abstract entered in Block 20, if different from Report)

18. SUPPLEMENTARY NOTES

paper presented at the Advanced Study Institute on the Physics and Chemistry of Low Dimensional Solids, Tomar, Portugal, August 1979

19. KEY WORDS (Continue on reverse side if necessary and identify by block number)

semiconducting $(CH)_x$; band structure; ~~density of states~~; optical absorption; visible and infrared reflectance; photovoltaic effect; p-n heterojunction; localized donor-acceptor states; semiconductor-metal transition; electron microscopy; conductivity; thermopower; magnetic susceptibility; Pauli susceptibility; Fermi surface; Kramers-Kronig analysis; tight binding approximation; mobility and transport

20. ABSTRACT (Continue on reverse side if necessary and identify by block number)

Linear polyacetylene, $(CH)_x$, is the simplest conjugated organic polymer and is therefore of special fundamental interest. Interest in this semiconducting polymer has been stimulated by the successful demonstration of doping with associated control of electrical properties over a wide range; the electrical conductivity of films of $(CH)_x$ can be varied over 12 orders of magnitude from that of an insulator ($\sigma \sim 10^{-9}$ ohm^{-1}cm^{-1}) through semiconductor to a metal ($\sigma \sim 10^{3}$ ohm^{-1}cm^{-1}). Various electron donating or accepting molecules can be used to yield n-type or p-type material, and compensation and junction formation have been demonstrated.

DD FORM 1 JAN 73 1473 EDITION OF 1 NOV 65 IS OBSOLETE S/N 0102-014-6601

Unclassified

SECURITY CLASSIFICATION OF THIS PAGE (When Data Entered)

ADA086869

DDC FILE COPY

80 7 18 061

19. semiconductor physics; device applications; Schottky barrier; photoelectrochemical photovoltaic cell; polyenes; optical anisotropy; solitons

20. Optical-absorption studies indicate a direct band-gap semiconductor with a peak absorption coefficient of about 3×10^5 cm^{-1} at 1.9 eV. Partial orientation of the polymer fibrils by stretch elongation of the $(CH)_x$ films results in anisotropic electrical and optical properties suggestive of a highly anisotropic band structure. The electrical conductivity of partially oriented metallic $[CH(AsF_5)_{0.1}]_x$ is in excess of 2000 $ohm^{-1}cm^{-1}$. The qualitative change in electrical and optical properties at dopant concentrations above a few percent have been interpreted as a semiconductor-metal transition by analogy to that observed in studies of heavily doped silicon. However, the anomalously small Curie-law susceptibility components in the lightly doped semiconductor regime indicate that the localized states induced by doping below the semiconductor-metal transition are nonmagnetic. These observations coupled with electron spin resonance studies of neutral defects in the undoped polymer have resulted in the concept of soliton doping; i.e. localized domain-wall-like charged donor-acceptor states induced through charge transfer doping.

OFFICE OF NAVAL RESEARCH

Contract N00014-75-C-0962

Task No. 356-602

TECHNICAL REPORT NO. 79-10

Conducting Organic Polymers: Doped Polyacetylene

by

A.J. Heeger[+] and A.G. MacDiarmid[≠]

Presented at

The Advanced Study Institute on the Physics and Chemistry
of Low Dimensional Solids
Tomar, Portugal
August 1979

Department of Physics[+] and
Department of Chemistry[≠]
Laboratory for Research on the Structure of Matter
University of Pennsylvania
Philadelphia, Pa. 19104

November 24, 1979

CONDUCTING ORGANIC POLYMERS: DOPED POLYACETYLENE

A. J. Heeger† and A. G. MacDiarmid‡

Laboratory for Research on the Structure of Matter
University of Pennsylvania, Philadelphia, PA 19104

Contents

† Dept. of Physics, U. of Pennsylvania
‡ Dept. of Chemistry, U. of Pennsylvania

I. INTRODUCTION

The electronic structure of polyenes has been a subject of interest for many years. The unsaturated bonds which characterize the polyenes have an important effect on their electronic structure and the corresponding electronic properties. In a polyene (see Fig. 1) three of the four carbon valence electrons are in sp^2 hybridized orbitals; two of the σ-type bonds are links in the backbone chain while the third forms a bond with some side group (e.g., H in Fig. 1). The remaining valence electron has the symmetry of the $2p_x$ orbital and forms a π bond in which the charge density is perpendicular to the plane of the molecule. In terms of an energy-band description, the σ bonds form low-lying completely filled bands, while the π bond would correspond to a half-filled band. The π bond could be metallic provided there is negligible distortion of the chain, and an independent-particle model proved to be satisfactory.

The possibility of a distortion of the molecular structure intrigued the early investigators. J. E. Lennard-Jones,[1] in an early application of Huckel theory of molecular orbitals, investigated the electronic structure of polyenes. His conclusion, that in the limit of an infinite chain the bonds tended to a constant value of 1.38 A, was later supported by studies of Coulson.[2] However, the theoretical conclusions seemed less than satisfactory in view of the experimental observations.[3] Using either molecular-orbital (MO) theory or a free-electron model in which the π electrons are considered free to delocalize along the chain, the energy for a transition to the lowest excited state decreases linearly with the reciprocal of the chain length. This rule was observed to work rather well for the short polyenes. However, experiments indicated that for very long chains the transition energy reached a limiting value of about 2 eV.[3] Later Kuhn[4] demonstrated that bond alternation could serve as a possible explanation of the energy gap in long polyenes.

The first convincing analysis was that given by Lounget-Higgins and Salem;[5] by assuming a well-defined model they were able to carry out the calculation without recourse to estimates of physical parameters. They found the uniform infinite chain unstable with respect to bond alternation. Hence for an infinite polyene the stable configuration is one of unequal bond lengths. This result is no more than a restatement of the one-dimensional (1-D) Peierls instability[6,7] for a special case. For long polyenes where bond alternation becomes important the electron is subject to a periodic potential with a period of twice the original undistorted chain. Such a potential introduces a gap at $2k_F$ causing a change of character in the polyene from a metal to a semiconductor.

The importance of correlation in long chain polyenes has

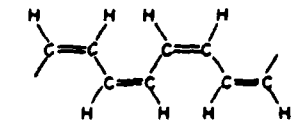

CIS

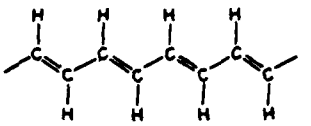

TRANS

Fig. 1. Molecular structure of cis and trans isomers of polyacetylene, $(CH)_x$.

been stressed by Ovchinnikov et al.[8] and others.[9] Ovchinnikov et al.[8] argued that the electronic gap of ~ 2 eV seen in the long chain polyenes is due almost entirely to correlation with the Peierls effect playing little or no part. However, there is not general agreement on this point. Grant and Batra[10] estimated a somewhat larger single particle energy gap, whereas Duke et al.[11] showed that a calculation including a combination of bond alternation and Coulomb interaction yields results in agreement with photoemission and optical absorption data.

Linear polyacetylene, $(CH)_x$, is the simplest conjugated organic polymer (Fig. 1) and is therefore of special fundamental interest in the context of the above discussion. From theoretical and spectroscopic studies of short chain polyenes, the π-system transfer integral can be estimated as $|t| \simeq 2\text{-}2.5$ eV. Such an estimate implies that the overall bandwidth would be of order 8-10 eV; $W_{\|} = 2Z|t|$. As a result of this large overall band width and unsaturated π-system $(CH)_x$ is fundamentally different from either the traditional organic semiconductors made up of weakly interacting molecules (e.g., anthracene, etc.), or from other saturated polymers with monomeric units of the form $(\underline{R}\text{-}\underline{C}\text{-}\underline{R})$ where there are no π-electrons (e.g., polyethylene, etc.). Polyacetylene is more nearly analogous to the traditional inorganic semiconductors. However, the transverse bandwidth due to interchain coupling is much less. The nearest-neighbor interchain spacing[12] of 4.39 Å implies a transverse bandwidth ($W_{\perp}$) comparable to the bandwidth (longitudinal) in molecular crystals like tetrathiafulvalenium-tetracyano-p-quinodimethanide (TTF-TCNQ);[7] thus $W_{\perp} \sim 0.1$ eV. Weak interchain coupling is therefore implied, and the system may be regarded as quasi-one-dimensional. Consequently, although the 1-D Peierls instability is not a full explanation of the electronic structure of polyacetylene, it provides a useful starting point of discussion for many of the electronic properties.

Interest in this semiconducting polymer has been stimulated by the successful demonstration of doping with associated control of electrical properties over a wide range;[13,14] the electrical conductivity of films of $(CH)_x$ can be varied over 12 orders of magnitude from that of an insulator ($\sigma \sim 10^{-9} \Omega^{-1} cm^{-1}$) through semiconductor to a metal ($\sigma \sim 10^{3} \Omega^{-1} cm^{-1}$).[15,16] Various electron donating or accepting molecules can be used to yield n-type or p-type material,[17] and compensation and junction formation have been demonstrated.[17,18] Optical-absorption studies[19] indicate a direct band-gap semiconductor with a peak absorption coefficient of about $3 \times 10^{5} cm^{-1}$ at 1.9 eV. Partial orientation[20] of the polymer fibrils by stretch elongation of the $(CH)_x$ films results in anisotropic electrical[21] and optical properties[19] suggestive of a highly anisotropic band structure. The electrical conductivity of partially oriented metallic $[CH(AsF_5)_{0.1}]_x$ is in excess of $2000 \Omega^{-1} cm^{-1}$.[21] The qualitative change in electrical and optical properties at dopant concentrations above a few percent have been interpreted as a semiconductor-metal transition[16] by analogy to that observed in studies of heavily doped silicon. However, the anomalously small Curie-law susceptibility[22] components in the lightly doped semiconductor regime indicate that the localized states induced by doping below the semiconductor-metal transition are nonmagnetic. These observations coupled with electron spin resonance studies of neutral defects[23,24] in the undoped polymer have resulted in the concept of soliton doping; i.e. localized domain-wall-like charged donor-acceptor states induced through charge transfer doping.[25,26]

The initial results obtained on conducting polymers have generated considerable interest from the point of view of potentially low cost solar energy conversion. Experiments utilizing polyacetylene, $(CH)_x$, successfully demonstrated rectifying junction formation.[17,18] In particular a p-$(CH)_x$:n-ZnS heterojunction solar cell has been fabricated with open circuit photovoltage of 0.8 Volts.[18] In related experiments, a photoelectrochemical photovoltaic cell was fabricated using $(CH)_x$ as the active photoelectrode.[27]

In this review, we will concentrate primarily on aspects of the work carried out at the University of Pennsylvania, bringing in contributions of colleagues at other institutions where appropriate. The focus will be on the fundamental physics and physical mechanisms. Detailed discussion of the more chemical aspects can be found elsewhere.[13,14]

II. SEMICONDUCTING $(CH)_x$

IIA. Band Structure[10,25]

As an initial approximation we consider a model in which the

π-electrons of trans-$(CH)_x$ are treated in a tight binding approximation and the σ electrons are assumed to move adiabatically with the nuclei. Let u_n be a configuration coordinate for displacement of the n^{th} CH group along the molecular symmetry axis (x), where u_n=0 for the undimerized chain. The Hamiltonian is

$$H = -\sum_{hs} (t_{n+1,n} c^{+}_{n+1,s} \; c_{n,s} + h.c.) + \sum_n \frac{K}{2}(u_{n+1}-u_n)^2 + \sum_n \frac{M}{2} u_n^2 \qquad (1)$$

where to first order in the u's,

$$t_{n+1,n} = t_o - \alpha(u_{n+1}-u_n). \qquad (2)$$

M is the mass of the CH unit, K is the spring constant for the σ energy when expanded to second order about the equilibrium undimerized systems, and c^{+}_{ns} (c_{ns}) creates (annihilates) a π electron of spin s on the n^{th} CH group. The band structure of the perfect infinite dimerized trans structure is shown in Fig. 2. In this perfect structure, the displacements are of the form

$$u_{no} = \pm (-1)^n u_o, \qquad (3)$$

where $\pm$ corresponds to the two possible degenerate structures (double bonds pointing "up" and double bonds pointing "down"). The transfer integrals for the perfect chain are

$$t_{n+1,n} = \begin{cases} t_o - t_1 & \text{"single" bond} \\ t_o + t_1 & \text{"double" bond} \end{cases} \qquad (4)$$

The overall bandwidth is $4t_o \simeq$ 8-10 eV; whereas the energy gap $Eg = 4t_1$ depends on the magnitude of the distortion. For example if $Eg = 4t_1 \simeq 1.4$ eV, the value of u_o which minimizes the ground state energy (assuming K = 10.5 eV/Å^2)[28] is u_o = 0.042 Å in the direction of the CH displacement while the bond length change due

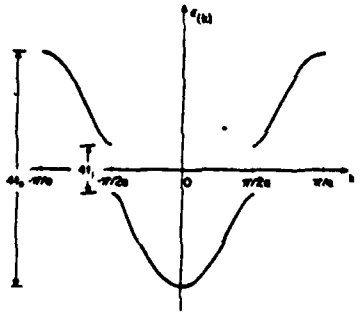

Fig. 2. Band structure of perfectly dimerized $(CH)_x$.

to bond alternation is $\sqrt{3}\ u_o = 0.073$ Å. Larger values of the energy gap require larger distortions; e.g. $E_g = 4t_1 = 2$ eV corresponds to $u_o = .056$ Å. In the presence of weak bond alternation with static distortion u_o

$$\mathcal{E}(k) = \pm 2\sqrt{t_o^2 \cos^2 ka + t_1^2 \sin^2 ka} \qquad (5)$$

where a is the c-c distance along the chain in the uniform structure. More detailed band calculations have been carried out by Grant and Batra[10] including consideration of the cis-structure and the effects of interchain coupling. The interchain coupling is expected to give transverse bandwidth of the order of a few tenths of an eV. Because of the crystal potential associated with the doubled unit cell of the cis-$(CH)_x$ structure, there is an energy gap even for uniform bonds. Consequently we expect the experimental energy gap for cis-$(CH)_x$ to be greater than that for trans-$(CH)_x$.

IIB. Optical Absorption[19,29,30]

Optical absorption data for trans-$(CH)_x$ and cis-$(CH)_x$ are shown in Figures 3a and 3b. The absorption coefficient for trans-$(CH)_x$ begins a slow increase around 1.0 eV rising sharply at 1.4 eV to a peak at about 1.9 eV. The magnitude of the absorption coefficient (3×10^5 cm^{-1}) at the peak is comparable with the peak value in typical direct gap semiconductors of about 10^5 cm^{-1}. For the cis isomer the absorption maximum is blue shifted by about 0.3 eV consistent with a somewhat larger gap.

A detailed analysis[29] of the absorption spectrum has been carried out in terms of the joint density of states for the optical interband transition. Using the tight-binding results discussed above and assuming weak interchain coupling the optical joint density of states takes the form sketched in Fig. 3c. The dashed curve represents the 1-D limit where the $(\delta-\delta_g)^{-\frac{1}{2}}$ singularity occurs at the band edge. Interchain coupling removes the singularity as described above shifting the maximum away from E_g^{direct} by an amount of order $W_\perp$. The possibility of an indirect gap, which may arise from interchain coupling, is indicated by extending the curve below E_g^{direct}.

Collecting these results we can make a qualitative picture of the optical absorption for a highly anisotropic (quasi-1-D) semiconductor. The optical absorption will begin once the photon energy is larger than the indirect gap and then increase rapidly to the quenched singularity, decreasing for larger photon energies. Such a picture agrees with the data for polyacetylene shown in Fig. 3. Taking the absorption peak to be 1.9 eV, one estimates the transverse bandwidth to be ≤ 0.5 eV. This value for $W_\perp \sim 2zt$ is consistent with the intermolecular transfer integrals in other

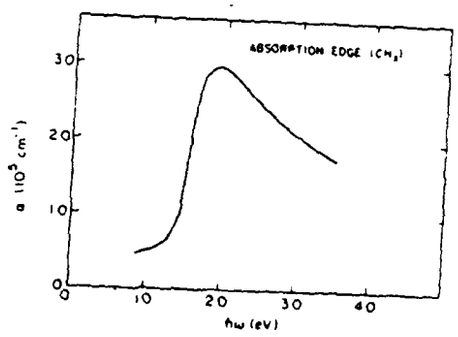

Fig. 3a. Absorption coefficient as a function of frequency; trans-$(CH)_x$ (ref. 29).

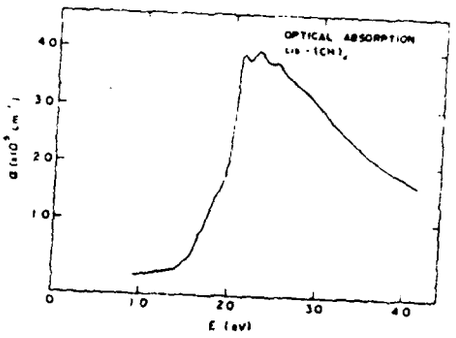

Fig. 3b. Absorption coefficient as a function of frequency; cis-$(CH)_x$ (ref. 29).

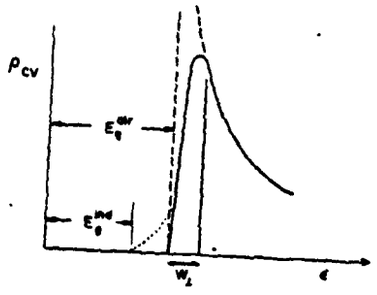

Fig. 3c. The joint optical density of states corresponding to the band structure of Fig. 10(a). The rounding of the square-root singularity arises from interchain coupling ($W_\perp$) (ref. 29).

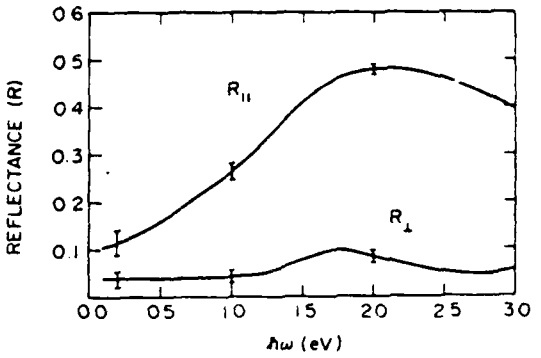

Fig. 4. Polarized reflectance as a function of frequency from partially oriented $(CH)_x$ (l/l_o=2.5). $R_{\parallel}$ and $R_{\perp}$ refer to light polarization parallel and perpendicular to the orientation direction (ref. 29).

molecular crystals such as TTF-TCNQ.[7] This interpretation of the optical absorption appears to be applicable to $(CH)_x$ as well as many other low-dimensional solids. Using the above analysis as a guide one would estimate from the data a direct gap of $\sim$1.4 eV.

IIC. Visible and Infrared Reflectance[21,29]

Figure 4 shows the polarized reflectance data from oriented films ($l/l_o \sim 2.5$-3) of pure trans-$(CH)_x$ where l_o and l are the unstretched and stretched lengths, respectively. The large optical anisotropy induced by orientation is clearly evident. The reflection data are consistent with a semiconductor model for pure $(CH)_x$ in qualitative agreement with the absorption data described above. The interband transition is apparent in $R_{\parallel}$ in the region of 2 eV with the reflectance decreasing to a low frequency value of $R_{\parallel} \simeq 0.1$, implying a dielectric constant of $\epsilon_{\parallel} \simeq 3$-4, in agreement with the value measured[31] at microwave frequencies (note that the low density of fibrils in the $(CH)_x$ films implies that the true value of $\epsilon_{\parallel}$ within a given fibril is $\epsilon \sim 10$-12). The perpendicular reflectance $R_{\perp}$ is small throughout the measured range indicative of quasi-one-dimensional behavior and relatively weak interchain coupling. The low frequency limiting value, $R_{\perp} \simeq 4\%$, implies $\epsilon_{\perp} \simeq 1.5$.

The Kramers-Kronig analysis was used to analyze the reflectance data for partially oriented pure trans-$(CH)_x$. The results for $\sigma_1(\omega)$ and $\epsilon_1(\omega)$ are presented in Figs. 5 and 6. The results are precisely as expected for a semiconductor; $\sigma(\omega)$ rises from zero at low frequencies to a peak value of $4 \times 10^3\ \Omega^{-1}\,cm^{-1}$ at about 16,000 cm^{-1}. $\epsilon(\omega)$ is negative at high frequencies crossing zero

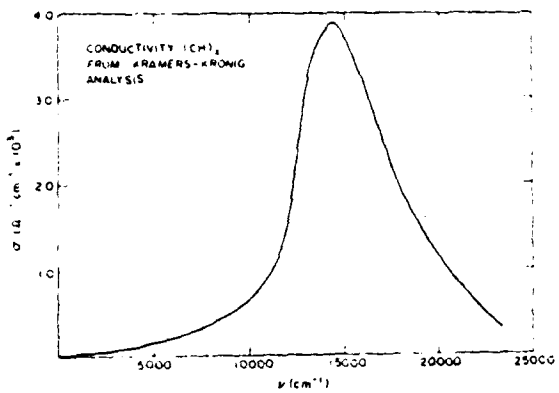

Fig. 5. $\sigma(\omega)$ for trans-$(CH)_x$ as obtained from Kramers-Kronig analysis of the $R_{||}$ reflection spectrum (ref. 29).

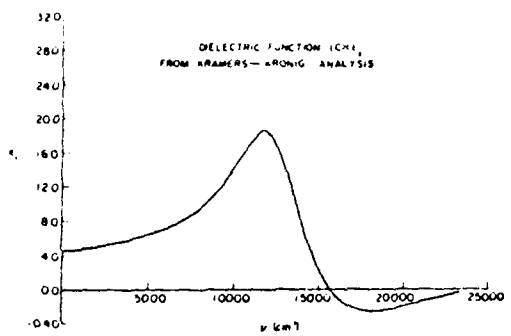

Fig. 6. $\epsilon(\omega)$ for trans-$(CH)_x$ as obtained from Kramers-Kronig analysis of the $R_{||}$ reflection spectrum (ref. 29).

at about 16,000 cm^{-1}. At low frequencies ϵ approaches a limiting value $\epsilon(o) \sim 4$ consistent with the values determined directly from $R(\omega \to 0)$ and the microwave data.

The absorption and reflection data are consistent and imply a semiconductor band structure with an energy gap arising from bond alternation of about 1.5 eV. However, as indicated in the introduction, this viewpoint is not universally accepted. Ovchinnikov et al.[8,9] have argued that the energy gap extrapolated to infinite chain polyenes is too large to be accounted for by simple band theory of the dimerized chain, and concluded that Coulomb correlations play an important role. It has been shown[32] that the gap due simultaneously to correlation and a Peierls dimerization is of the form $\Delta \approx (\Delta^2_{corr} + \Delta^2_{alt})^{\frac{1}{2}}$. Various other theoretical

studies have shown that Coulomb correlation may be important in this system. Duke et al.[11] use a CNDO-S2 calculation scheme on polyenes of varying lengths, $C_{4n+1}H_{4n+2}$ (n = 1,2,3,4) to find an approximation to the band structure, electron photoemission spectra, and the lowest electronic transition energy. Using a configuration interaction analysis, Duke et al.[11] also conclude the lowest B_uMO. The energy difference is then the lowest singlet molecular exciton. The exciton band is then extrapolated to $n \rightarrow \infty$ in order to predict the transition energy in polyacetylene, obtaining $\Delta E \simeq 2.0$ eV. The agreement between the extrapolated value and the experimental absorption edge is quite good.

The optical data appear consistent with either of two models for the electronic structure of polyacetylene. The first view is simple single-particle (band theory) point of view, while the second view models $(CH)_x$ as a strongly correlated system where single-particle ideas are invalid. Since excitons may be viewed as bound electron-hole pairs, whereas a direct π-π^* transition would create a free electron and hole, direct observation of electron-hole pair generation through photoconductivity and/or photovoltaic studies is of critical importance.

IID. Photovoltaic Effect[18,27,33]

Photovoltaic studies have been carried out using trans-$(CH)_x$: n-ZnS heterojunctions, photoelectrochemical cells using $(CH)_x$ as the active photoelectrode, and Schottky barriers formed with Indium metal on $(CH)_x$.[33] The photoresponse of the trans-$(CH)_x$: n-ZnS heterojunction diode is shown in Fig. 7. One sees two photoresponse edges, at approximately 1.4 eV and 2.6 eV. The magnitude of the peak at 0.9 eV was dependent upon previous illumination and thus probably arises from trapping states in the gap. The data therefore are consistent with optical studies of $(CH)_x$ which imply a gap energy of about 1.5 eV. However, the relatively low quantum efficiency below 2.5 eV may indicate primary exciton formation. Thus the actual single particle energy gap may be somewhat higher than 1.5 eV. Under illumination of approximately 1 sun, the $(CH)_x$:ZnS heterojunction gives an open circuit photovoltage of 0.8 V.

Photoelectrochemical photovoltaic cells have been fabricated[27] using polyacetylene, $(CH)_x$, as the active photoelectrode. Using a sodium polysulfide solution as electrolyte, $V_{oc} \simeq 0.3$ Volts and $I_{sc} \simeq 40$ μ amps/cm^2 were obtained under illumination of approximately 1 sun. With the initial configuration, the cell efficiency was limited by the series resistance, the small effective area of the electrode configuration, and the absorbance of the solution. The PEC photoresponse falls rapidly at photon energies below 1.4 eV, consistent with optical studies of $(CH)_x$ which suggest a band gap energy of about 1.5 eV. However, again, the relatively low

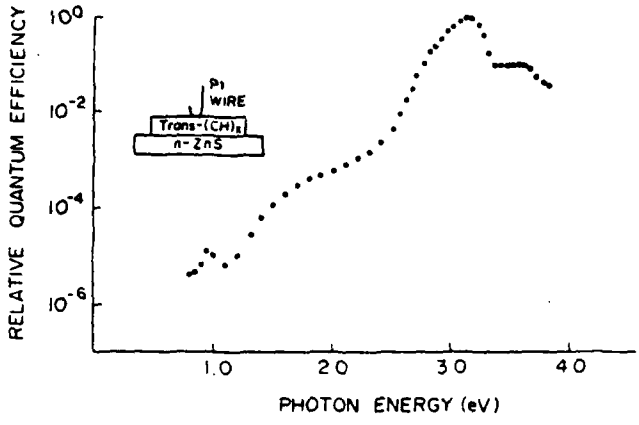

Fig. 7. Photoresponse of n-ZnS:undoped trans-$(CH)_x$ n-p heterojunction. Quantum efficiency normalized to 3.1 eV peak where the absolute quantum efficiency is of order unity. (ref. 18).

quantum efficiency below 2.5 eV may indicate primary exciton formation.

In summary, optical absorption and reflection data are consistent with the band structure of a direct gap semiconductor with an energy gap of about 1.5 eV. Photovoltaic response is observed with an onset near 1.5 eV. However, the relatively low quantum efficiency strongly suggests that the true single particle band gap is somewhat higher with the edge at 1.5 eV being due to a weakly bound exciton.

III. DOPING OF $(CH)_x$[13-17,34]

When pure polyacetylene is doped with a donor or an acceptor, the electrical conductivity increases sharply over many orders of magnitude at low concentration, then saturates at higher dopant levels, above approximately 1%. The maximum conductivity for nonaligned cis-$[CH(AsF_5)_{0.14}]_x$ is in excess of $10^3\ \Omega^{-1}\text{-cm}^{-1}$ with similar values obtained for a variety of dopants. The typical behavior for the conductivity as a function of dopant concentration (y) is shown in Figure 8. The general features appear to be the same for the various donor and acceptor dopants, but with detailed differences in the saturation values and the critical concentration at the "knee" in the curve (above which σ is only weakly dependent on y). These transport studies suggest a change in behavior at a critical concentration (y_c); a semiconductor to metal (SM) transition.

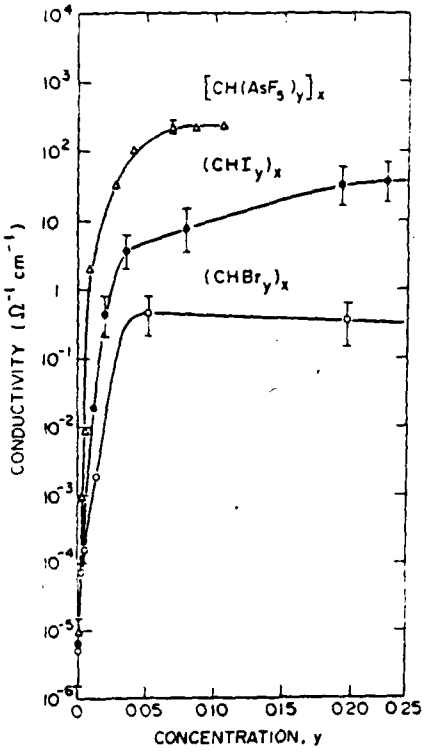

Fig. 8. Electrical conductivity (room temperature) as a function of dopant concentration.

IIIA. Localized Donor/Acceptor States: Light Doping

The simplest model of the localized donor or acceptor state at light doping ($y < y_c$) follows the traditional semiconductor approach and pictures the electron or hole, with effective mass m^* determined by the band structure loosely bound to the charged center by Coulomb forces in a dielectric medium. In lightly doped $(CH)_x$, instead of substitutionally replacing the host as in silicon, the impurity resides very close to the polymer chain, on the surface of the 200 Å fibrils and/or between individual chains. At light doping levels we assume isolated impurities interacting with a single polymer chain. At heavy doping levels impurity interactions will become important, however, well below the SM transition this should not be a problem. The impurity could either donate an electron to, or accept an electron from the chain. In the acceptor case, the hole on the chain would be free to delocalize if it were not for the Coulomb binding to the impurity. The resulting localized states are bound states of the hole on the polymer chain in the vicinity of the charged donor or acceptor ion. The binding energies of such quasi-one-dimensional hydrogenic

impurity states have been shown to be the same as for donors and acceptors in traditional semiconductors.[31] Note that these hydrogenic bound states will contain one electron or hole with spin $\frac{1}{2}$ and thus will give a Curie-law contribution to the magnetic susceptibility.

The assumption that charge transfer doping leads to electrons and holes assumes a rigid band structure along the lines of traditional semiconductor physics. However, as discussed in IIA, the bond-alternation energy gap in trans-$(CH)_x$ may be viewed as the result of the $2k_F$ instability of the coupled electron-lattice system in a quasi-1d metal. In this point of view, the effect of charge-transfer doping would be to change $k_F = (\pi/2)n$, where n is the number of carriers per unit length along the chain in the undistorted metallic state. In the pure polymer, there is one electron per carbon atom corresponding to a half-filled band so that $n_o = a^{-1}$, where a is the uniform carbon-carbon bond length and $k_F = k_F^o = \pi/2a$. The resulting charge-density-wave distortion occurs with a superlattice period $b_s^o = 2\pi/2k_F = 2a$, implying a dimerized bond-alternating structure as observed in $(CH)_x$. Doping will change k_F; $k_F = (\pi/2)n_o(1 \pm c)$, where c is the impurity concentration, and the plus or minus sign is appropriate for donor or acceptor doping. We have assumed complete charge transfer. The resulting superlattice period will shift away from $b_s^o = 2a$ to a new value $b_s = 2a/(1 \pm c)$, incommensurate with the carbon-chain polymer structure. However, the commensurability energy strongly favors locking $2k_F$ at the zone boundary; a commensurate bond alternation with period 2a places π-bond charge between carbon atoms [Fig. 10(a)], whereas in the incommensurate case, the charge-density maxima and minima would not be related to the atomic positions. As a compromise the doped structure breaks up into domains; i.e. regions of bond-alternation separated by charged domain walls.

The formation of domain-walls, or solitons, on long chain polyenes has been studied theoretically by Su, Schrieffer and Heeger,[25] and by Rice.[26] Following their work, we consider two domains with B phase to the left and A phase to the right of a soliton which is at rest at the origin, as illustrated in Fig. 9a. To determine the properties of the soliton (width, energy, mass, spin, etc.) the ground state energy of the system was determined for an arbitrary displacement pattern which reduces to the A and B phases as one moves to the far right or left. In practice, the displacements were varied in a segment containing N CH groups located symmetrically about n=0, and matched onto perfect A and B phases on either side. The ground state energy was then calculated for any set of displacements, u_n, in the segment. Defining the staggered order parameter $\Psi_n = (-1)^n u_n$ (which reduces to $\pm u_o$ for the A and B phases and is zero by symmetry at the center of the wall), and choosing as a trial function

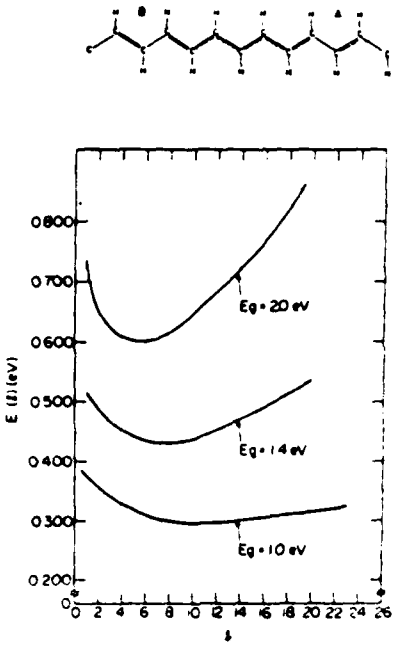

Fig. 9 (ref. 25).
a. Schematic of soliton separating A and B phases.
b. Soliton energy as a function of wall width for three values of Eg.

$$\Psi_n = u_o \tanh(\frac{n}{\ell}) \tag{7}$$

the system energy $E(\ell)$ was determined as shown in Figure 9b for $4B_1$ = 1.0, 1.4, and 2.0 eV. The minimum occurs at $\ell \simeq 7$ for $4B_1$ = 1.4 eV so that the wall is quite diffuse (for $4B_1$ = 2.0 eV, $\ell \simeq 5$ and for $4B_1$ = 1.0 eV, $\ell \simeq 9$). The energy to create the soliton at rest is $E_s \simeq 0.4$ eV for the 1.4 eV gap energy (0.6 eV for $4t_1$ = 2.0 eV, 0.3 eV for $4t_1$ = 1.0 eV). Using the adiabatic approximation for the electronic motion, it was shown that the effective mass of the soliton is related to the δu_n for a small change in wall position δx_s by

$$M_s = M \sum_n \left(\frac{\delta u_n}{\delta x_s}\right)^2 \simeq \frac{4u_o^2 M}{3\ell a^2}, \tag{8}$$

where the second equality holds if we use (7) and replace n by $n-x_s/a$ in the derivative. Using the values obtained above for $4t_1$ = 1.4 eV, one finds $M_s \simeq 6\ m_e$, where m_e is the electron mass.

The electronic structure of the soliton exhibits a localized

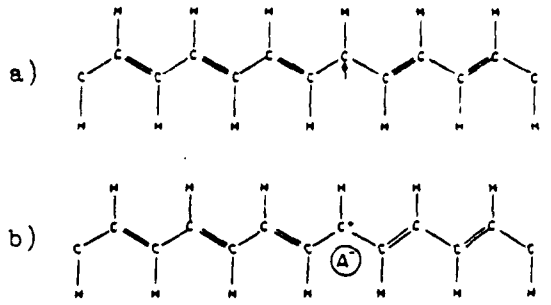

Fig. 10. a. Neutral soliton defect in trans-$(CH)_x$ (paramagnetic).
b. Soliton kink after charge transfer (diamagnetic).

state φ_0 at the center of the gap, containing one electron for the neutral kink. While this localized state is spin unpaired, the distorted valence band continues to have spin zero. Thus, the neutral soliton has spin $\frac{1}{2}$. The static susceptibility therefore will contain a Curie law contribution and can be used to count the number of soliton defects present.

Since the localized state occurs at the gap center, i.e. the chemical potential, the relevance of the solitons to the doping of $(CH)_x$ depends on the energy for creation of a soliton, E_s, as compared with the energy required for making an electron or a hole, $\frac{1}{2} E_g = \Delta$. If $\Delta < E_s$, charge transfer doping would occur by creating free band excitations; if $\Delta > E_s$, soliton formation would be favored. For $E_g = 1.4$ considered above, $E_s \simeq 0.4$ eV $< \Delta = 0.7$eV. Thus, the soliton bound hole leads to stabilization over the free hole by $(\Delta - E_s) \simeq 0.3$ eV with correspondingly larger values if the gap is larger. The same stabilization energy holds for adding an electron, which would occupy $\varphi_0(x)$ of the soliton rather than being placed at the conduction band edge. Self consistent field effects arising from electron-electron interactions would split the ionization and affinity levels of φ_0 about the center of the gap and change these estimates accordingly. We note that the ionized solitons formed upon doping with acceptors (or donors) will be non-magnetic.

The origin of the localized state can be seen from elementary chemical arguments. Fig. 10a shows a schematic diagram of a neutral kink localized on a single lattice site. Satisfying the carbon valence at the center of the kink requires a non-bonded pi-electron ($S=\frac{1}{2}$) localized on the kink (Fig. 10a). Ionization by a nearby acceptor leads to a charged, non-magnetic, kink (Fig. 10b). For simplicity the kinks are shown localized on one lattice

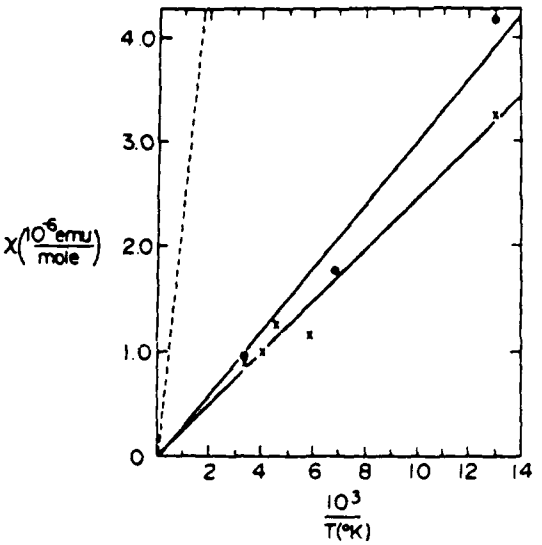

Fig. 11. Spin susceptibility of nonmagnetic $(CH)_x$ ooo undoped sample. xxx $[CH(AsF_5)_{0.006}]_x$. Both samples were from same batch of undoped polymer. The dotted line represents the Curie law expected for y=0.006 assuming AsF_5^- with spin $\frac{1}{2}$ (ref. 22).

site whereas minimization of the energy will spread the kink over many sites as described above.

An important difference between the conventional semiconductor doping (electrons or holes bound in the Coulomb potential of the ion) and soliton doping is the magnetic character of the resulting localized states. Because of the spin degeneracy of a single hole (or electron) in a localized state, the magnetic susceptibility would be expected to obey a Curie law. Double occupancy of such weakly bound states in the gap is inhibited by electron-electron Coulomb interactions. On the other hand, the charged ionized soliton localized state is diamagnetic.

Experimental studies[22] have shown that the localized states induced by doping are non-magnetic in agreement with the soliton theory outlined above. For example, a series of electron spin resonance measurements (10 GHz) were carried out on a sample lightly doped (y=0.006) with AsF_5 and an undoped trans-$(CH)_x$ as shown in Fig. 11. Both samples exhibited Curie-like susceptibilities between 77 K and 295 K. Assuming $S = \frac{1}{2}$ for the observed spins, the concentrations of unpaired local moments are 850 and 630 per 10^5 carbon atoms for y=0 and 0.006, respectively. The local-moment concentration in undoped trans-$(CH)_x$ is roughly consistent with previous measurements by Shirakawa[23] and Goldberg

et al.[24] of $300/10^6$ carbon atoms. Differences are probably due to minor variations in film preparation and isomerization. Significantly, however, the trans-$(CH)_x$ showed no enhanced local-moment concentration upon doping. Shown also in Fig. 11 (dashed line) is the Curie-law susceptibility which would correspond to one unpaired spin generated per AsF_5 for $y = 0.006$. From these results one concludes that the localized states induced by light doping below the SM transition are non-magnetic. This result was confirmed by Faraday balance measurements. The residual weak Curie law from defects in the undoped $(CH)_x$ decreases in magnitude as y increases rather than increasing in proportion to the dopant concentration.

Other evidence relevant to the soliton question is summarized by Su, Schrieffer and Heeger[25] and by Fincher, Ozaki, Heeger and MacDiarmid.[31] Although considerable work needs to be done in this area, the experimental results are in qualitative agreement with the soliton doping mechanism.

IIIB. Semiconductor-Metal Transition and the Metallic State

The semiconductor-metal transition in doped polyacetylene has been studied by a variety of experimental techniques including electrical conductivity, thermopower, magnetic susceptibility, far-ir transmission, and ir reflectance; all as a function of dopant concentration. In general qualitative changes are evident in essentially all the physical properties, indicative of semiconductor behavior below y_c and metallic behavior above y_c where y_c is about 0.03 (i.e. $\sim$ 3 mole% dopant).

i) Transport: Conductivity[14,15] and Thermopower[35]. Typical data for electrical conductivity (room temperature) as a function of dopant concentration are shown in Fig. 8. The change in behavior above $\sim$ 3% is evident. Similar changes are observed in the temperature dependence; samples with $y < y_c$ show activated behavior with the activation energy decreasing with increasing dopant concentration. For $y > y_c$, the activation energy is sufficiently small that the interfibril contacts play a limiting role.

Since thermoelectric power is a zero-current transport coefficient, thermopower measurements can provide important information on such a system. The interfibril contacts should be unimportant allowing an evaluation of the intrinsic metallic properties. Moreover, since the thermopower (S) can be viewed as a measure of the entropy per carrier, measurements as a function of y can be used to study the SM transition. One generally expects a large thermopower for semiconductors (few carriers with many possible states per carrier) whereas in the metallic state the entropy of the degenerate electron gas is small ($\sim k_B(k_BT/E_F)$ per carrier).

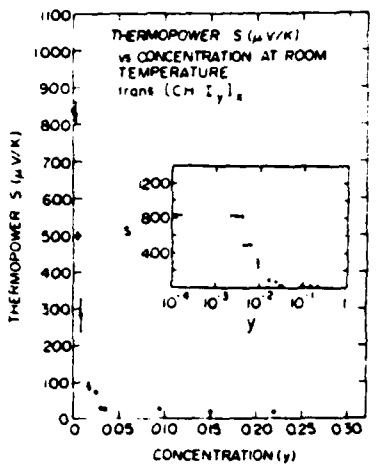

Fig. 12. Thermopower of (CHI_y) as a function of iodine concentration y. The inset shows the data with y on a log scale; the value for undoped $(CH)_x$ is indicated with an arrow (ref. 35).

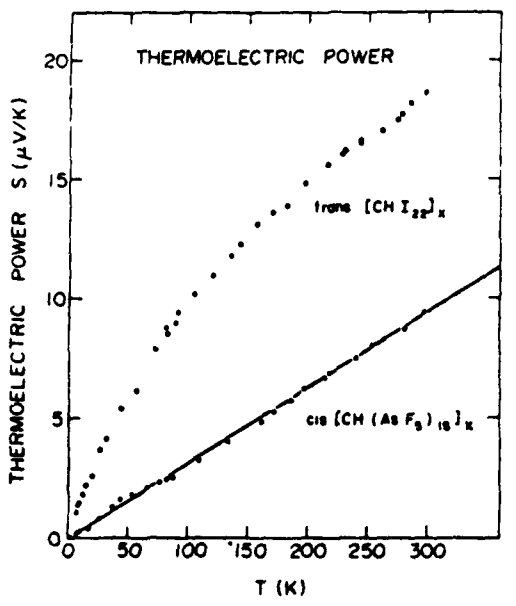

Fig. 13. Temperature dependence of the thermopower for heavily doped metallic $(CH)_x$.

Thermopower studies were carried out by Park et al.[35] The room temperature results, S vs y for trans-$(CHI_y)_x$ are shown in Fig. 12. The sign of S is positive throughout the entire concentration range indicating p-type behavior consistent with charge transfer doping to the iodine acceptor and the formation of I_3^-. The metal insulator transition is clearly evident. Note that S remains constant up to approximately y = 0.003 (0.3%) (see inset) then falls steeply for $0.003 < y < 0.03$. Above 3 mole %, S is nearly independent of y decreasing to S = +18.5μV/K in the heavily doped metallic limit. From this change in behavior, we infer a critical concentration, $n_c \simeq 3$ mole% (1 mole% I_3^-), for the semiconductor-metal transition in $(CHI_y)_x$. Below 0.3%, the thermopower is insensitive to the dopant implying that the transport is dominated by defects and/or impurities in the synthesized trans-polymer.

The thermopower in the metallic high concentration limit is shown in Figure 13 where S vs T is plotted on a linear scale. Figure 13 includes the results for both trans-$(CHI_{0.22})_x$ and trans-$[CH(AsF_5)_{0.15}]_x$. The results for the AsF_5 doped sample are in excellent agreement with those obtained by Kwak et al.[36] S is a linear function of T whereas for the iodine doped sample, there is somewhat more curvature (in eq. 9 we have written the result in units of $(k_B/e) = 86\mu V/K$ where k_B is the Boltzmann constant, and $|e|$ is magnitude of the electron charge). In both cases, the thermopower decreases smoothly toward zero as $T \rightarrow 0$ in a manner typical of metallic behavior. The magnitude and temperature dependence of S (Fig. 13) are characteristic of a degenerate electron gas. Thus the TEP results independently verify the metallic state above y_c and thereby confirm that the temperature dependent conductivity (decreasing with decreasing temperature) is limited by interfibril contacts; i.e. interrupted metallic strand behavior.

For a nearly filled band (i.e. p-type) metallic system, the thermopower can be written as

$$S = +\frac{\pi^2}{3}\left(\frac{k_B}{|e|}\right) kT \left[\frac{d\ell n\sigma(E)}{dE}\right]_{E_F} \qquad (9)$$

where $\sigma(E) = n(E)|e|\mu(E)$ and n(E) is the number of carriers contributing to $\sigma(E)$, $dn(E)/dE = g(E)$ is the density of states (both signs of spin) and $\mu(E)$ is the energy dependent mobility. Assuming energy independent scattering ($\mu(E)$ independent of E)

$$S = +\left(\frac{k_B}{|e|}\right)\frac{\pi^2}{3} k_B T_\eta \, (E_F) \qquad (10)$$

where $\eta(E_F) = g(E_F)/N$ is the density of states per carrier. The experimental results (Fig. 13) are in good agreement with eq. 10; the results imply $\eta(E_F) = 1.36$ states per eV per carrier. Since there are 0.15 carriers per carbon atom in $[CH(AsF_5)_{0.15}]_x$

(assuming complete charge transfer), the thermopower data yield for the density of states, $g(E_F) \simeq 0.2$ states per eV per C atom. The curvature and somewhat larger values found for the $(CHI_{0.22})_x$ data may imply an additional contribution arising from energy dependent scattering.

For dilute concentrations well below the semiconductor-metal transition the thermopower is large and essentially temperature independent. Such behavior can be understood for a dilute concentration of carriers (holes) which hop among a set of localized states. In this case, where the kinetic energy of the carriers is negligible, the thermopower is given by the Heikes formula[37,38]

$$S = + \frac{k_B}{|e|} \ell n[(1-\rho)/\rho] \qquad (11)$$

where $\rho = n/N$ is the ratio of the number of holes (n) to the number of available sites (N) (eq. 11 assumes spinless Fermions; the inclusion of spin degeneracy changes the expression to $S = +(k_B/|e|)\ell n(2-\rho)/\rho$). Identification with the experimental data for undoped <u>trans</u>-$(CH)_x$ requires that $\rho \sim 10^{-4}$ and temperature independent. The results therefore suggest that in the undoped polymer, the conductivity is due to a small number of residual carriers ($\rho_o \sim 10^{-4}$) provided by defects and/or impurities, and that the mobility results from hopping. The insensitivity of the thermopower to iodine concentrations less than 0.3 mole% (or 0.1% I_3^-) is consistent with this interpretation and implies that $\rho_o < 10^{-3}$. Moreover, the large TEP together with $\rho_o \sim 10^{-4}$ implies that the number N of available sites is comparable to the number of carbon atoms per unit length in the polymer chain.

The localized state hopping transport inferred from the thermopower measurements below y_c is consistent with the soliton doping mechanism. Motion of the charged localized domain-walls would be expected to be via diffusive hopping. Moreover, for a fixed impurity concentration the number of charged kinks would be independent of temperature in agreement with the data for undoped $(CH)_x$ and for dopant concentration $y < y_c$. Finally, although the domain wall would be distributed over a group of carbon atoms, in the dilute limit the center of mass of the wall could take any position along the chain so that the number of available sites would be of order the number of carbon atoms.

ii) <u>Magnetic Susceptibility.</u>[22] The magnetic properties of a material can provide important details of its electronic structure. In the heavily doped samples, a temperature-independent paramagnetic contribution to the susceptibility suggests the existence of a degenerate Fermi sea of metallic charge carriers. From the Pauli formula the Fermi-surface density of states $N(E_F)$ may be obtained; $\chi_p = \mu_B^2 N(E_F)$, where μ_B is the Bohr magneton and

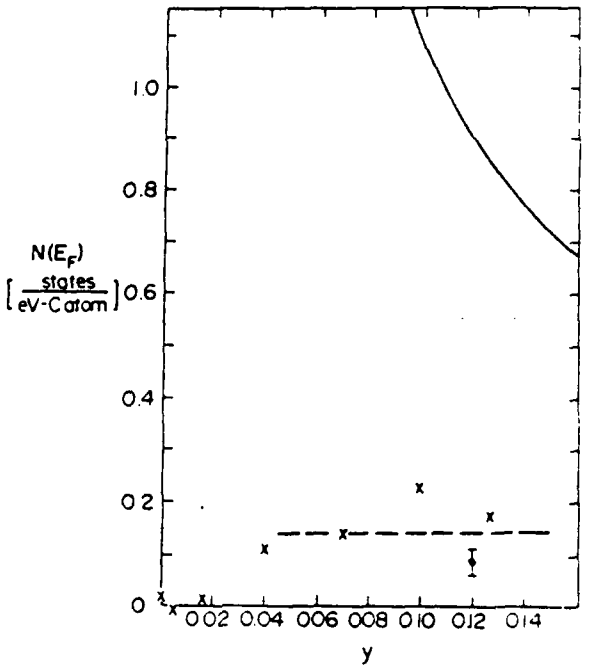

Fig. 14. Fermi-surface density of states vs AsF_5 concentration. The solid curve represents a rigid band one-dimensional density of state ($m^*/m = 1$). The dashed curve would result from a half-filled simple tight-binding band with transfer integral t = 2.25 eV (bandwidth of 9 eV). x Faraday balance; • ESR (see ref.22).

$N(E_F)$ includes both spin directions. The onset of such a temperature-independent Pauli term in the susceptibility as a function of dopant concentration indicates the transition from the semiconducting to the metallic state.

Magnetic susceptibility studies have been carried out as a function of dopant concentration in $[CH(AsF_5)_y]_x$. The measured total susceptibilities for all samples studied were diamagnetic indicating the dominance of atomic core contributions.

Treating the paramagnetic deviation from the prediction of Pascal's constants as a Pauli susceptibility, the Fermi-surface density of states $N(E_F)$ is obtained

$$\chi_{meas} - \chi_{Pascal} = \mu_B^2 N(E_F) \qquad (12)$$

These results are plotted in Fig. 14. The density of states in the metallic regime, $N(o) \simeq 0.15$ states/eV/carbon atom, is in

excellent agreement with that inferred from the thermopower.

Anisotropies found in the electrical[21] and optical[19] properties of partially oriented films suggest that heavily doped polyacetylene may be described as a quasi-one-dimensional metal. Theoretical one-dimensional band structures predict a divergence in the density of states at the band edge. Plotted in Fig. 14 for comparison is the Fermi-surface density of states for $[CH(AsF_5)_y]_x$ in a one-dimensional rigid-band model assuming $m^*/m = 1$ and one free hole generated per AsF_5. Clearly, the experimental results give no indication of such a one-dimensional band-edge anomaly.

A possible explanation of this result is that above the SM transition bond alternation and the associated energy gap no longer exist. That is, the band structure is that of a one-dimensional metal with a half-filled conduction band. The dashed line in Fig. 14 represents a calculation of $N(E_F)$ for such a half-filled band in a simple tight-binding model with transfer integral 2.25 eV. Raman spectra[39] of metallic iodine doped $(CH)_x$, however, continue to show the two absorption bands identified with C=C and C-C stretching modes with only minor frequency shifts compared with the pure polymer. Moreover, optical absorption and reflection data imply that the interband transition is present above the SM transition. Thus bond alternation persists into the metallic regime. On the other hand, x-ray photoemission studies indicate nonuniform doping at the highest concentrations.[40] An inhomogeneous metallic state with undistorted metallic domains coexist with regions of bond-alternated semiconductor is consistent with the data.

Alternatively, the small density of states may result from interchain coupling. Although the interchain distance is even greater than the intermolecular distances in molecular crystals such as TTF-TCNQ, it has been suggested that even this small amount of three-dimensional coupling is sufficient to quench the one-dimensional band-edge divergence in the density of states.[10]

The Pauli susceptibility of $[CH(AsF_5)_y]_x$ seems to turn on continuously at AsF_5 concentrations of a few atomic percent. Within the limits of experimental uncertainty the susceptibility of $[CH(AsF_5)_{0.04}]_x$ is temperature independent (77-295 K). Therefore, the results of this work provide no evidence of strong correlation enhancement of the spin susceptibility near the SM transition.

iii) Infrared Absorption and Reflection.[16,41,42] To verify the existence of the semiconductor-to-metal transition, far infrared transmission data were taken on samples of varying concentrations of iodine and AsF_5 (with qualitatively similar results).

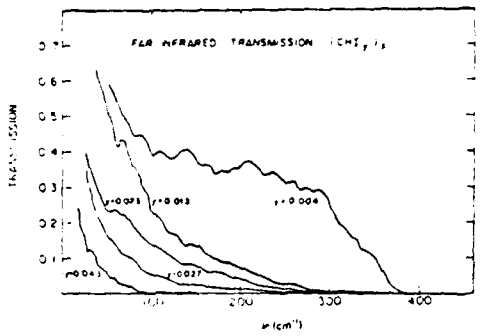

Fig. 15. Infrared transmission through $(CHI_y)_x$ films (ref. 41).

The data[16,41] for a series of iodinated samples with $y \rightarrow y_c$ are shown in Fig. 15. At all frequencies the transmission decreases with increasing concentration. As $y \rightarrow y_c$, the far ir transmission cuts off at progressively longer wavelengths consistent with an approach to metallic behavior. Results for $y \rightarrow 0.05$ are not shown because the transmission level is less than the amount of scattered light ($\sim 1\%$) in the apparatus.

Since the long wavelength reflectance is particularly sensitive to the free carrier density, the ir reflection spectra demonstrate, with special clarity, the occurrence of the semiconductor-metal transition and to the formation of the metallic state. The results indicate that the critical concentration range is 1-3% in agreement with the values inferred from dc transport, far ir transmission, thermopower and magnetic studies. The anisotropy of the polarized reflectance implies that the free carrier contribution is polarized along the polymer chains.

The reflectance results obtained from oriented $(CH)_x$ films doped with AsF_5 are shown in Figure 16. The error bars are indicative of the variations obtained from different samples separately prepared and mounted. Figure 16 contains data for $[CH(AsF_5)_y]_x$ with y = 0, 0.006, 0.034, 0.093 and 0.134. Since the transition from semiconductor to metal occurs at AsF_5 concentration of about 1-3%, the data of Figure 16 span the full concentration range. Metallic behavior is clearly indicated at the highest concentrations; the reflectance increases with decreasing frequency with a value approaching 90% at the longest wavelengths. On the other hand for light doping ($y < 0.01$) the reflectance remains small even at the longest wavelength consistent with semiconducting behavior. The sharp increase in reflectance below 0.2 eV in the y = 0.034 sample is indicative of the presence of free carriers; evidently this sample is close to the boundary between semiconductor and metal.

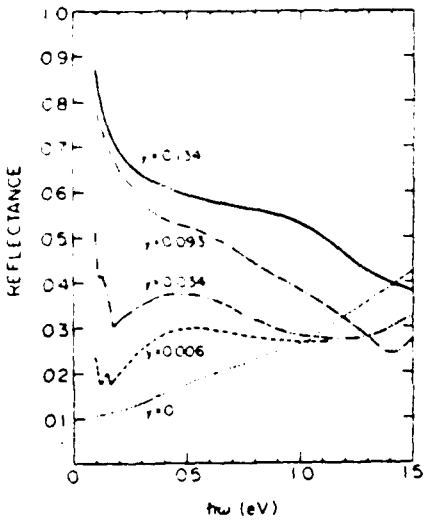

Fig. 16. Reflectance ($R_{\parallel}$) for oriented $[CH(AsF_5)_y]_x$ (ref. 42).

The broad reflectance peak centered near 0.5 eV is evident for both the AsF_5 doping (Fig. 16) and the iodine doping. For light doping a well-defined maximum is observed suggesting the introduction of states within the energy gap. At higher levels the 0.5 eV band grows in strength with an increasingly long, low frequency tail. Qualitatively the 0.5 eV maximum which shows up at the lightest doping levels appears to evolve continuously into the free carrier reflectance in the metallic regime. Evidently the states introduced into the gap at low doping grow in number (the magnitude of R) and in length (the low frequency cut-off) as the doping level increases. The series of spectra suggest an interpretation in terms of small metallic regions which gradually grow and coalesce into an extended metallic state at the highest doping concentrations.

iv) Kramers-Kronig Analysis of Metallic $[CH(AsF_5)_{0.13}]_x$.[29] A Kramers-Kronig transform has been carried out to analyze the reflectance data (0.1 eV-3.0 eV) of metallic $[CH(AsF_5)_{0.13}]_x$. At the lowest frequencies (Fig. 16), the data were extrapolated to approach unity as $\nu \rightarrow 0$ assuming a Hagen-Rubens behavior of the reflectance below 0.1 eV. Because the results of a Kramers-Kronig transform are very sensitive in the far infrared to the precise manner in which $R(\omega) \rightarrow 1$ as $\omega \rightarrow 0$, an accurate determination of $\sigma(\omega)$ in this frequency region is extremely difficult. However, it was found that in the middle ir (above 1500 cm^{-1}) $\sigma(\omega)$ is insensitive to the details of the low frequency extrapolation. The results for $\sigma(\omega)$ are shown in Fig. 17. The broad peak in $\sigma(\omega)$ centered around 16,000 cm^{-1} results from the interband

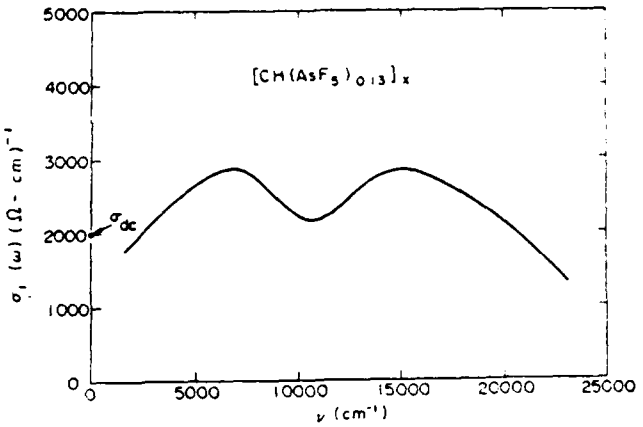

Fig. 17. $\sigma_{||}(\omega)$ for heavily doped metallic $[CH(AsF_5)_{0.11}]_x$ as obtained from the $R_{||}$ reflection spectrum (ref. 29).

transition. The conductivity then begins to fall at lower frequencies until 11,000 cm^{-1}, where it again rises as one might expect for a system with free carriers. However, a somewhat surprising result is that below 6000 cm^{-1} the conductivity again decreases. This behavior is markedly different from the simple Drude behavior where $\sigma(\omega)$ is a monotonically decreasing function of frequency [$\sigma_{Drude} = \sigma_o/(1+\omega^2\tau^2)$]. The slow drop in $\sigma(\omega)$ continues until 1500 cm^{-1}, which is the lower limit of the analysis. Between 1000 and 1500 cm^{-1} a weak dependence on the low frequency extrapolation was observed with the behavior below 1000 cm^{-1} strongly dependent upon the extrapolation. Above 1500 cm^{-1} the results are independent of the extrapolation except for minor adjustments of the values in the third or fourth significant digit, details beyond the resolution of this analysis. The value $\sigma_{dc} \simeq 2\times10^3\,\Omega^{-1}\,cm^{-1}$ found through direct dc measurements on heavily doped (AsF_5) oriented samples of $(CH)_x$ is indicated in Fig. 17. Thus, the low frequency limit of this Kramers-Kronig analysis is quite consistent with other independent measurements. The decrease of σ below 6000 cm^{-1} is a real feature of $\sigma(\omega)$ and not an artifact of the extrapolation procedure.

Useful information can be extracted by applying the sum rule relations to the data from the metallic state (Fig. 17). The effective number of electrons per molecule participating in the free-carrier optical transitions for energies less than the interband transition is given by the oscillator strength

$$8\int_0^{\omega_c}\sigma(\omega)d\omega = \frac{4\pi Ne^2}{m^*}\,\eta_{eff}(\omega_c), \qquad (13)$$

where $n_{eff}(\omega_c)$ is the fractional number of carriers contributing to the metallic conductivity. Using $\nu_c = 11{,}000\ cm^{-1}$, we find the oscillator strength ($\simeq 4 \times 10^{21}$) approximately equal to the total π-electron oscillator strength in the polymer. The large oscillator strength therefore suggests that heavy doping removes the bond-alternation leading to a uniform bond length polyene; a quasi-one-dimensional broad band metal with all π electrons contributing to the transport, i.e., $n_{eff} \simeq 1$. Such a picture is consistent with the small value of the density of states at E_F as inferred from magnetic susceptibility[22] and thermopower[35] studies. On the other hand, after doping, Raman data continue to show the two carbon-carbon stretch frequencies[39] (diminished in intensity), and optical studies[19,29] continue to show evidence of the unshifted interband transition (no Burstein shift), both characteristic of the bond alternated semiconductor. A possible explanation is an inhomogeneous metallic state (possibly resulting from inhomogeneous doping within the fibrils[40]) with undistorted metallic domains coexistent with regions of bond alternated semiconductor. Such a picture is consistent with all the data and explains the apparent absence of a Burstein shift upon doping, the residual Raman lines, and the observed sensitivity of the strength of the interband transition (after doping) to the different dopants.

The low frequency decrease in $\sigma(\omega)$ extrapolating toward the dc value cannot be understood in terms of a simple Drude-Lorentz model of the conductivity. However, it is intuitively clear that the fibril nature of the polymer will have a very strong effect on the dc transport properties. Moreover, if the metallic system is highly anisotropic on a microscopic scale as suggested by dc and optical studies of partially oriented films, impurities and defects will have an especially strong effect; in one dimension disorder leads to localization of states. Thus we anticipate that the low frequency transport will be limited by the imperfect polymer structure.

Electron microscopy[21,23,43] photographs of $(CH)_x$ films show a fibril structure with fibril diameter of about 200 Å. The individual fibrils form a multiply coupled array through branching. Typical length to diameter ratio for the fibrils appear to be in the range of about 5-10. Therefore the polymer can be viewed as an effective medium made up of $(CH)_x$ fibrils at a volume filling factor of about $f = \frac{1}{3}$. For the as-grown films, the fibrils are randomly oriented in the plane; stretch orientation leads to partial alignment. From examination of the electron micrographs and related x-ray data[44] we estimate approximately 75% alignment, i.e., the alignment factor, $\alpha \simeq 0.75$.

Within the doped $(CH)_x$ metallic fibrils the intrinsic frequency-dependent conductivity and dielectric functions are denoted $\sigma_1(\omega)$ and $\epsilon_1(\omega)$. The bulk properties of the metallic polymer can be

related to $\sigma_1(\omega)$ and $\epsilon_1(\omega)$ through effective-medium theory (see ref. 29). The average medium conductivity can be written

$$\langle\sigma_1(\omega)\rangle \simeq \frac{\alpha f \sigma_1(\omega)}{\overline{1}+[4\pi\sigma(\omega)/\omega]^2 g^2(1-\alpha f)^2} \qquad (14)$$

where f is the filling factor, α is the fractional alignment factor, and g is the typical depolarization factor ($g = (b/a)^2 [\ln(2a/b)-1]$) for an ellipsoid of revolution, where b/a is the ratio of minor to major semiaxes. In writing the above expression, we have assumed that, consistent with the metallic behavior, $4\pi\sigma_1/\omega > |\epsilon_1|$. Moreover, as a result of the observed dc and optical anisotropy, we consider only the response to components of the applied field parallel to the $(CH)_x$ fibrils.

The important feature of Eq. 14 is that at low enough frequencies, the electric field within an "interrupted strand" is screened by the depolarization field due to the charge buildup at the boundary. The characteristic cutoff frequency ω_c is given by

$$[4\pi\sigma_1(\omega_c)/\omega_c]g(1-\alpha f) = 1 \qquad (15)$$

and corresponds to the condition when the depolarization factor in the denominator of Eq. 14 exceeds unity. From Fig. 17, we estimate $\omega_c \sim 7000\ cm^{-1}$ at which point the (maximum) medium conductivity is approximately $3\times10^3\,\Omega^{-1}cm^{-1}$. Taking $\alpha f \sim 0.25$ as described above, Eq. 15 yields $g \sim 10^{-2}$, or $b/a \sim 10^{-1}$, in good agreement with the fibril morphology. The results therefore imply that the fibril structure of $(CH)_x$ leads to metallic polymers which may be viewed as interrupted metallic strands. From the magnitude of the cutoff frequency we infer strand dimensions consistent with fibril dimensions observed in electron microscopy studies. Therefore the interrupted strands are tentatively identified with the branched fibrils; localization due to microscopic disorder appears to be relatively unimportant in these crystalline polymers.

An estimate of the intrinsic conductivity within the individual metallic doped $(CH)_x$ fibrils can be obtained by inverting eq. 14. At ω_c, the denominator is ~ 2, so that assuming $\alpha f \simeq \frac{1}{4}$, we find $\sigma_1(\omega_c) \simeq 2.4\times10^4\,\Omega^{-1}cm^{-1}$. The intrinsic dc conductivity is undoubtedly higher. If we assume a Drude dependence, $\sigma_1(\omega) = \sigma_0/(1+\omega^2\tau_0^2)$, where τ_0 is the Drude scattering time for the metallic state. It is difficult to obtain a direct measurement of τ_0 from the available data. However, the decrease in $\langle\sigma_1(\omega)\rangle$ observed from 7000 to 11,000 cm^{-1} in Fig. 14 implies that $\omega_c\tau_0 > 1$. Thus from this analysis we are able to estimate the intrinsic dc conductivity within a single fibril of metallic $(CH)_x$; $\sigma^{dc}_{intrinsic} \geq 2 \times 10^4\,\Omega^{-1}cm^{-1}$.

v) Mobility Changes at the SM Transition. Direct measurements of the mobility (e.g. time of flight, etc.) are not available.

Hall effect data[45] have been reported in the metallic regime; however, the Hall coefficient appears to be dominated by the fibril structure of the composite medium. Some information on the transport mobility in the semiconductor and metal limits can be obtained directly from the conductivity, $\sigma = ne\mu$ where n is the density of carriers with charge e, and μ is the mobility.

In the undoped trans-$(CH)_x$, the thermopower results imply a carrier concentration of 10^{-4} resulting from residual impurities, defects, etc. Thus, since the number of carbon atoms per unit volume is $n_c \simeq 2 \times 10^{22} cm^{-3}$ (based on the measured density of 0.4 grams/cm^3), the residual carrier density in undoped trans-$(CH)_x$ is $\sim 10^{18} cm^{-3}$. With $\sigma \simeq 10^{-5} \Omega^{-1}\text{-}cm^{-1}$ (see Fig. 3), one finds $\mu(\text{undoped}) \simeq 10^{-4} cm^2/V\text{-}sec$.

In the metallic regime, e.g. $[CH(AsF_5)_{0.1}]_x$ the numbers of carriers can be estimated from the oscillator strength (see subsection iv above). The results imply that in the heavily doped metallic state all the π-electrons contribute to the metallic transport; thus $n(\text{metal}) \simeq 2 \times 10^{22} cm^{-3}$. Taking the intrinsic conductivity to be $\sigma_{\text{intrinsic}}^{1c} \sim 2 \times 10^{4} \Omega^{-1}\text{-}cm^{-1}$ as inferred above, one obtains $\mu(\text{metal}) \simeq 10\ cm^2/V\text{-}sec$. Note that assuming that all π-electrons contribute requires that heavy doping removes the bond-alternation (see subsection iv above) leading to a uniform bond length polyene. Taking a somewhat more conservative point of view one could estimate the number of carriers by assuming unit charge transfer with one carrier per dopant. For $[CH(AsF_5)_{0.1}]_x$, the corresponding value would be $n \sim 2 \times 10^{21}$ with $\mu \sim 10^2 cm^2/V\text{-}sec$!

The high mobility in the metallic state provides strong evidence of the validity of a band theory approach with delocalized states in this disordered metallic polymer. The inferred values of μ are comparable to or greater than the mobilities in the best metals (e.g. for copper $\mu \sim 50\ cm^2/V\text{-}sec$ at room temperature).

The low mobility inferred for the undoped polymer and the remarkable increase on going through the SM transition are surprising. The low mobility in undoped $(CH)_x$ is, however, consistent with the thermopower results which imply hopping in the undoped polymer. Hopping transport is not expected for electrons or holes in a broad band (w~8-10 eV) system unless strong electron-lattice coupling leads to large effective mass carriers. The soliton doping mechanism discussed above (Sec. IIIA) does lead to relatively large effective mass, e.g. $M_s \sim 6m_e$ for Eg = 1.4 eV, $M_s \sim 12\ m_e$ for Eg = 2.0eV. Thus the low mobility is consistent with soliton formation induced by charge transfer doping. Of course, more conventional polaron effects and/or disorder localization could also play a role.

The low mobility inferred indirectly from the dc transport may not be appropriate to optically induced electron-hole pairs

particularly when generated in the high electric field of a junction. Such optically induced minority carriers would move rapidly to the interface and out of the polymer before a kink could form. Thus, the optically induced carrier mobilities may be comparable to the band-like values found in the metallic regime ($\mu \sim 10$-100 cm^2/V-sec). This important question can only be resolved by more direct measurements involving photogenerated carriers.

vi) The Mechanism of the SM Transition. As an initial point of view we treated this transition as similar to that seen in heavily doped semiconductors. In this case, one expects the halogen and AsF_5 dopants to act as acceptors with localized hole states in the gap, with the hole bound to the acceptor in a hydrogen-like fashion. For low concentrations, one expects the combination of impurity ionization and variable range hopping to lead to a combination of activated processes as observed experimentally. However, as extensively discussed by Mott[46] and others,[97] if the concentration is increased to a critical level, then the screening from carriers will destroy the bound states giving an insulator-to-metal transition. This will occur when the screening length becomes less than the radius of the most tightly bound Bohr orbit of the hole and acceptor in the bulk dielectric;

$$n_c^{\frac{1}{3}} \simeq (4a_H)^{-1} \left(\frac{m^*}{m\epsilon}\right) \tag{16}$$

where a_H is the Bohr radius, ϵ is the dielectric constant of the medium and m^*/m is the ratio of the band mass to the free electron mass. Assuming $m^*/m \simeq 1$ and using $\epsilon \simeq 10$ from ir reflection measurements, we estimate $n_c \sim 10^{20}$-10^{21} cm^{-3}. Since the density of carbon atoms is about $2 \times 10^{22} cm^{-3}$, n_c would be in the range of a few percent assuming one carrier per dopant. The good agreement with our experimental results is probably fortuitous in view of the much over-simplified model. More importantly, the magnetic properties of doped $(CH)_x$ are inconsistent with the SM transition being a Mott transition in the conventional sense. There are two important points of disagreement:

1) The localized states at light doping are non-magnetic (see Sec. IIIA).
2) There is no evidence of strong correlation enhancement of the Pauli susceptibility near the SM transition (see Sec. IIIBii and Fig. 14).

Thus the SM transition in doped polyacetylene is fundamentally different from that observed in traditional semiconductors where 1) and 2) above play a central role.

As shown above, the optical-ir reflectance data suggest an interpretation in terms of small metallic regions which gradually grow and coalesce into an extended metallic state at the highest doping concentrations. In addition, the oscillator strength

analysis (Sec. IIIBiv) leads to the conclusion that all the π-electrons contribute to the metallic conductivity suggesting that heavy doping removes the bond alternation leading to uniform bond length metallic trans-$(CH)_x$. This is consistent with the small density of states inferred from χ and TEP studies. In the context of the soliton doping mechanism discussed above, this picture of the SM transition could be at least qualitatively understood. Isolated charged solitons would be non-magnetic, in agreement with experiment. An attractive interaction between solitons would lead to a coalescence into uniform bond-length metallic regions. As the dopant density increases, the metallic regions would begin to overlap giving, eventually, a metallic state. A naive estimate of the critical concentration would be $y_c = 1/2N$ where N is the hald-width of the soliton; taking $N \simeq 7$ one obtains $y_c \simeq 6\%$. Inclusion of interchain coupling could lead to a percolation threshold at lower values. The interpretation of the SM transition as arising from soliton-soliton interactions has been considered in more detail recently by Rice,[48] Schrieffer[49] and Horowitz.[50] This interesting possibility will undoubtedly stimulate further theoretical and experimental [illegible].

IV. SEMICONDUCTOR PHYSICS AND DEVICE APPLICATIONS[17,18,27]

A variety of rectifying junctions have been fabricated using doped and undoped $(CH)_x$. Schottky diodes formed between metallic AsF_5-doped $(CH)_x$ and n-type semiconductors indicate high $[CH(AsF_5)_y]_x$ electronegativity. The p-type character of undoped trans-$(CH)_x$ is confirmed by Schottky barrier formation with low work function metals. An undoped p-$(CH)_x$:n-ZnS heterojunction has been demonstrated with open circuit photovoltage 0.8 V. These results point to the potential of $(CH)_x$ as a photosensitive material for use in solar cell applications.

As an example, the I-V and C-V characteristics of a Schottky junction formed with n-GaAs: (metallic)$[CH(AsF_5)_y]_x$ are shown in Fig. 18. The interface was fabricated by direct polymerization of the $(CH)_x$ film on the semiconductor surface. Several n-GaAs: (metallic)$[CH(AsF_5)_y]_x$ diodes were produced. As indicated by C-V and J-V characteristics, all had barrier heights in the range 0.8-1.0 V consistent with results for most metal: n-GaAs interfaces. Photosensitive diodes were fabricated using thin semi-transparent $[CH(AsF_5)_y]_x$ films. Illumination through the polymer with a tungsten lamp produced open circuit voltages in the range 0.4-0.6 V.

The formation of rectifying Schottky junctions has been demonstrated with undoped trans-$(CH)_x$ as the semiconductor. Metal contacts to the $(CH)_x$ films were formed by pressing small area metal tips onto polymer films in inert atmosphere. The undoped polymer forms ohmic contacts with highly electronegative metals

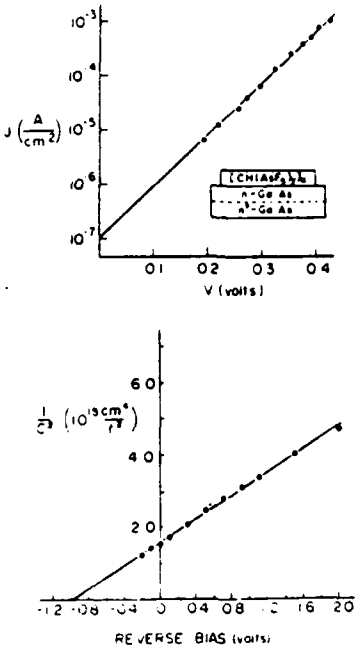

Fig. 18.

(Cu, Au, Pt) and rectifying junctions (Schottky diodes) with relatively low electronegativity metals (Na, Ba, In). The systematically different behavior with metals of different electronegativity shows that undoped trans-$(CH)_x$ is a p-type semiconductor consistent with thermopower data.

A p-n heterojunction was produced[18] from undoped trans-$(CH)_x$: n-ZnS as shown in the inset of Fig. 7. Both free standing films (pressure contact) and thin film polymerization of $(CH)_x$ directly on the n-ZnS single crystal were employed to form the interface. In each case rectifying junctions were obtained. The data (Fig. 7) indicate significant photoresponse at energies well below the 3.7 eV ZnS band gap; the peak absolute efficiency occurring at 3.1 eV is ~ 0.003. This result is clearly a severe underestimate of the actual photogeneration efficiency due to inefficient collection of photocarriers by the small area point contact. Capacitance measurements imply that the active area of the $(CH)_x$:ZnS diode was confined to a small region around the point contact and was far smaller than the entire 0.15 cm^2 interface area. To quantify this the following experiments were carried out: Junction capacitance was measured on the original cell and, subsequently, after doping with AsF_5 to reduce the series resistance. The $(CH)_x$ film was then removed, and replaced over the identical area by a sputtered Au contact, and the capacitance was measured. The junction capacitance of the $(CH)_x$:ZnS diode was < 20 pf, whereas

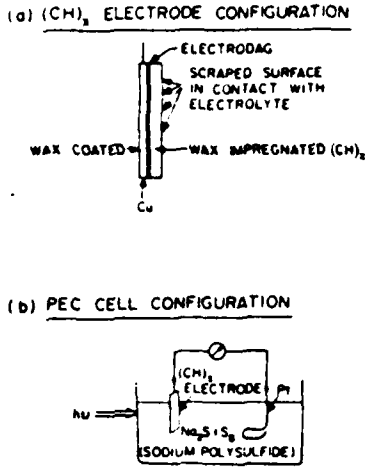

Fig. 19.

after doping with AsF_5, the capacitance increased to ~ 10 nf. The junction capacitance of the Au:ZnS diode was also ~ 10 nf. Therefore an area correction to the quantum efficiency of order 10^2-10^3 is implied leading to an actual quantum efficiency for the $(CH)_x$:n-ZnS junction approaching unity at 3.1 eV. Evidently, this represents photoactivation of carriers in $(CH)_x$ since such a photoresponse from ZnS at a photon energy 0.6 eV below its band gap with light illuminating the junction through ~1 mm of ZnS is not reasonable.

Photoelectrochemical photovoltaic cells[27] have been fabricated using polyacetylene as the active photoelectrode. Utilization of polyacetylene as a photoelectrode in a photoelectrochemical (PEC) cell offers attractive prospects. In general, semiconductor-electrolyte junctions are relatively insensitive to the quality of the semiconductor and are favored over solid state junctions with regard to trapping and surface recombination. The porous fibrillar microstructure of semiconducting $(CH)_x$ should be an advantage in PEC cells since the electrolyte can come into effective contact with the large surface area (~ 40 m^2/g). Since photoexcitation of polyacetylene involves only pi-electrons with the backbone binding sigma-bond remaining intact, photodissolution may not be a serious problem.

The $(CH)_x$ electrode configuration utilized is shown in Fig. 19. To reduce series resistance, the $(CH)_x$ film is contacted to a thin copper sheet using Electrodag. The entire structure is then dipped into molten paraffin wax; the wax is subsequently partially removed from the active surface by scraping with a razor blade thus exposing only the outermost fibrils to the electrolyte. The wax-filled electrode was utilized in these

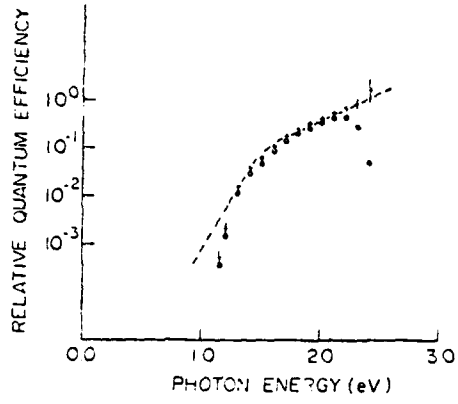

Fig. 20.

initial studies as a simple means of preventing permeation of the electrolyte through the porous film to the Electrodag backing.

The aqueous electrolyte consisted of a saturated Na_2S solution to which sulfur has been added to saturation. The alcohol/water electrolyte consisted of either a) 1 volume of saturated aqueous sodium polysulfide and two volumes of isopropyl alcohol to which sulfur has been added to saturation, or b) 1 volume of the saturated aqueous sodium polysulfide solution to which 1 volume of isopropyl alcohol has been added. The resulting sodium polysulfide solution acts as an effective redox couple

$$S_y^{-2} + 2e^- \rightleftharpoons S_{y-n}^{-2} + S_n^{-2} \qquad (y \geq n+1)$$

Since $(CH)_x$ is p-type, photogenerated electron-hole pairs are separated at the $(CH)_x$-electrolyte interface with electrons injected into the electrolyte. The resulting $S^=$ ions migrate to the Pt electrode where they lose electrons to reform the $S_y^=$ species. The liberated electrons return to the $(CH)_x$ electrode via the external circuit. Since $(CH)_x$ is hydrophobic, the alcohol was added to the solution to achieve improved contact at the $(CH)_x$ surface.

The photoresponse spectrum of the $(CH)_x$ PEC cell is shown in Fig. 20 plotted as relative quantum efficiency vs photon energy. The open circles represent data obtained directly from the cell with light incident on the photoelectrode through the highly colored orange solution which rapidly becomes opaque above 2.2 eV. The crosses represent the quantum efficiency corrected for light absorption by the electrolyte. The absolute quantum efficiency is approximately 1% at 2.4 eV. The dashed curve on Fig. 20 represents[51] the photoconductivity response of $(CH)_x$ (normalized to

the PEC cell data at 2 eV) as measured at the University of Pennsylvania using standard techniques. The nearly identical shapes of the PEC photoresponse and the $(CH)_x$ photoconductivity curves indicate that the former arises from electron-hole generation in the semiconducting polymer with subsequent minority carrier (electron) transfer into the sodium polysulfide solution at the interface.

In a general context, these junction formation experiments demonstrate that doped $(CH)_x$ can be used in a manner similar to conventional semiconductors. The Fermi level can be set (and moved) by selected dopants. Photogeneration of carriers has been demonstrated both in solid state p-n and Schottky junctions and in the PEC configuration. Quantum efficiencies are low below 2 eV but increase to values approaching unity at higher energies.

V. PROGRESS ON NEW MATERIALS

Considering possible polyacetylene derivatives, replacement of some or all of the hydrogen atoms in $(CH)_x$ with organic or inorganic groups, copolymerization of acetylene with other acetylenes or olefins, and the use of completely different conjugated polymers, a large new class of conducting organic polymers can be anticipated with electrical properties that can be controlled over the full range from insulator to semiconductor to metal. Work along these lines has been initiated. Substituted polyacetylene derivatives are being studied at a number of laboratories with initial results that look promising. The work on poly(para-phenylene)[52] and polypyrrole have demonstrated a second system which can be doped (n- and p-type) etc. with resulting properties similar to those of doped $(CH)_x$.

Continuing collaborative work[53] at the U. of Massachusetts and the U. of Pennsylvania, and independent studies of Shirakawa[54] in Tokyo have resulted in the synthesis of a new form of polyacetylene with variable density, through the isolation of a gel as a synthetic intermediate step. Scanning electron micrographs show the fibril structure characteristic of $(CH)_x$, but with a fibril diameter of ~ 600 Å to 800 Å. Electrical conductivity and thermopower measurements on samples of the undoped polymer and on samples doped with iodine or AsF_5 imply properties nearly identical with previously studied as-grown films of $(CH)_x$, but with a lower density of $(CH)_x$ fibrils per unit volume.

The density of the "foam-like" materials was in the range 0.02 gm/cm^3 to 0.04 gm/cm^3 with some variation from sample to sample. Pressed films were obtained with density 0.1 gm/cm^3 to 0.4 gm/cm^3 depending on the final thickness. These values are to be compared with the 0.4 gm/cm^3 density of the as-grown $(CH)_x$

films. Since the flotation density of the as-grown $(CH)_x$ film is 1.2 gm/cm^3, the volume filling fraction, f, of fibrils is approximately 1/3. For the "foam-like" material, $f \sim 0.015$ - 0.03 whereas the variable thickness pressed films have intermediate values for f.

Electrical conductivity and thermopower data were obtained from the "foam-like" material and from pressed films. Measurements were carried out on undoped samples and on samples heavily doped with iodine or AsF_5. The thermopower of the undoped polymer is insensitive to the density; the "foam-like material and the pressed film yield thermopower values of approximately +900 μV/K. Any variations are comparable with the typical variations observed earlier in as-grown film samples from different synthetic preparations. Similarly, after heavy doping, the results are insensitive to the density with values for the "foam-like" material, pressed film and as-grown films in good agreement for each dopant. Comparison with the variation in S as a function of dopant concentration studied in detail earlier leads to the conclusion that the heavily doped samples are all metallic. The thermopower results imply that the various forms of the doped and undoped polymers are microscopically identical. The low density materials simply consist of fibrils at a smaller filling fraction, f.

The electrical conductivity data are consistent with this conclusion. The conductivity of the undoped "foam-like" material is nearly two orders of magnitude below that of the high density pressed film. Although there may be some increase in the interfibril contact resistance, the reduction in f is of major importance. This conclusion is strengthened by the observation that the conductivity activation energy (obtained from the temperature variation of the conductivity near room temperature) is 0.25 eV for both samples. This value is comparable to the 0.3 eV value typically obtained from as-grown films.

Similar results are obtained with the heavily doped polymers. The conductivity (176 $ohm^{-1}-cm^{-1}$) of the $[CH(AsF_5)_{0.06}]_x$ prepared from the low density pressed cis-$(CH)_x$ film (ρ = 0.1 gm/cm^3) is correspondingly lower than that of the conductivity (560 $ohm^{-1}-cm^{-1}$, 1200 $ohm^{-1}-cm^{-1}$) of $[CH(AsF_6)_{0.14}]_x$, $[CH(AsF_5)_{0.10}]_x$, respectively, prepared from as-grown cis-$(CH)_x$ film (ρ = 0.4 gm/cm^3). The room temperature conductivity of $(CHI_{0.08})_x$ increases by a factor of forty on going from the low density "foam-like" materials to the high density pressed film. In all cases, the resulting conductivity increases with the filling fraction of fibrils. Note that the increased fibril size in the "foam-like material and pressed films does not appear to significantly alter the resulting transport properties of the doped polymers. The resulting doped and undoped variable density $(CH)_x$ polymers can be viewed as effective media in which the dc electrical transport is determined by the volume filling fraction of conducting fibrils.

VI. CONCLUSION

The emergence of polyacetylene as a prototype conducting organic polymer can be viewed in the context of the recent developments in research on quasi-1d organic conductors. In only a few years, organic conductors have progressed from tiny, brittle, molecular crystals with single crystal electrical conductivity less than 10^{2} $(\Omega\text{-cm})^{-1}$ to large area flexible $(CH)_x$ polymer films with conductivity systematically controllable over a remarkable range (less than $10^{-13}\Omega^{-1}\text{-cm}^{-1}$ to greater than $2\text{x}10^{3}\Omega^{-1}\text{-cm}^{-1}$. The interest in the fundamental physics and chemistry of this novel system and the initial success in device fabrication have stimulated a broad based interdisciplinary study of doped conducting polymers in many laboratories throughout the world. New concepts, new materials, and new and unusual electronic properties have already been demonstrated. It appears safe to conclude that this field will continue to grow; and that by means of a three fold interdisciplinary effort involving chemistry, physics and polymer science, conducting polymers will develop into a broad class of materials of considerable scientific interest and potential technological importance.

REFERENCES

1. Lennard-Jones, J. E.: 1937, Proc. R. Soc. A 158, p. 280.
2. Coulson, C. A.: 1938, Proc. R. Soc. A 164, p. 383.
3. Brooker, L. G. S.: 1951, J. Am. Chem. Soc. 73, p. 1087; 73, p. 5332.
4. Kuhn, H.: 1948, Helv. Chim. Acta 31, p. 1441.
5. Lounget-Higgins, H. C. and Salem, L.: 1959, Prov. R. Soc. A 25, p. 172.
6. Peierls, R. E.: 1955, "Quantum Theory of Solids" (Oxford University, London), Chap. 5.
7. "Low Dimensional Cooperative Phenomena", edited by H. J. Keller (Plenum, New York, 1975); "Chemistry and Physics of One Dimensional Metals", edited by H. J. Keller (Plenum, New York, 1977); "One Dimensional Conductors", edited by J. Devreese (Plenum, New York, 1978).
8. Ovchinnikov, A. A., Ukrainski, I. I., and Kventsel, G. V.: 1978, Usp. Fiz. Nauk. 108, p. 81 [Sov. Phys. Usp. 15, p. 575 (1978)].
9. Szabo, A., Langlet, J., and Malriev, J.: 1976, Chem. Phys. 13, p. 173; Cojan, C., Agrawal, G. P. and Flytzanis, A.: 1977, Phys. Rev. B 15, p. 909; Kertez, M., Koller, J., and Azman, A.: 1977, J. Chem. Phys. 67, p. 1180.
10. Grant, P. M. and Batra, I. P.: 1979, Solid State Commun. 29, p. 225.
11. Duke, C. B., Paton, A., Salaneck, W. R., Thomas, H. R., Plummer, E. W., Heeger, A. J. and MacDiarmid, A. G.: 1978, Chem. Phys. Lett. 59, p. 146.

12. Hsu, S., Signorelli, A., Pez, G., and Baughman, R.: 197[illegible] J. Chem. Phys. 68, p. 5105; 69, p. 106.
13. Heeger, A. J. and MacDiarmid, A. G., Proc. of the Dubrovn. Conf. on Quasi One-Dimensional Conductors, p. 361. Lecture Notes in Physics 96, Ed., S. Barisic (Springer-Verlag Berl. Heidelberg New York, 1979); MacDiarmid, A. G. and Heeger, A. J., "Molecular Metals", Ed. W. Hatfield, NATO Conference Series VI: Materials Science, (Plenum Press, New York and London, 1979), p. 161. See also accompanying paper in this volume by A. G. MacDiarmid and A. J. Heeger for more details on chemical aspects of the problem.
14. Shirakawa, H., Louis, E. J., MacDiarmid, A. G., Chiang, C. K., and Heeger, A. J.: 1978, Chem. Commun. p. 578; Chiang, C. K., Druy, M. A., Gau, S. C., Heeger, A. J., Shirakawa, H., Louis, E. J., MacDiarmid, A. G. and Park, Y. W.: 1978, J. Am. Chem. Soc. 100, p. 1013.
15. Chiang, C. K., Park, Y. W., Heeger, A. J., Shirakawa, H., Louis, E. J., and MacDiarmid, A. G.: 1978, J. Chem. Phys. 69, p. 5098.
16. Chiang, C. K., Fincher, C. R., Jr., Park, Y. W., Heeger, A. J., Shirakawa, H., Louis, E. J., Gau, S. C., and MacDiarmid, A. G.: 1977, Phys. Rev. Lett. 39, p. 1098.
17. Chiang, C. K., Gau, S. C., Fincher, C. R., Jr., Park, Y. W., MacDiarmid, A. G., and Heeger, A. J.: 1978, Appl. Phys. Lett. 33, p. 181.
18. Ozaki, M., Peebles, D., Weinberger, B. R., Chiang, C. K., Gau, S. C., Heeger, A. J. and MacDiarmid, A. G.: 1979, Appl. Phys. Lett. 35, p. 83.
19. Fincher, C. R., Jr., Peebles, D. L., Heeger, A. J., Druy, M. A., Matsumura, Y., MacDiarmid, A. G., Shirakawa, H., and Ikeda, S.: 1978, Solid State Commun. 27, p. 489.
20. Shirakawa, H. and Ikeda, S. (to be published).
21. Park, Y. W., Druy, M. A., Chiang, C. K., Heeger, A. J., MacDiarmid, A. G., Shirakawa, H., and Ikeda, S.: 1979, Polymer Lett. 17, p. 195.
22. Weinberger, B. R., Kaufer, J., Heeger, A. J., Pron, A., and MacDiarmid, A. G.: 1979, Phys. Rev. B 20, p. 223.
23. Shirakawa, H., Ito, T., Ikeda, S.: 1978, Die Macromolecular Chemie 179, p. 1565.
24. Goldberg, I. B., Crowe, H. R., Newman, P. R., Heeger, A. J., and MacDiarmid, A. G.: 1979, J. Chem. Phys. 70, p. 1132.
25. Su, W. P., Schrieffer, J. R., and Heeger, A. J.: 1979, Phys. Rev. Lett. 42, p. 1698.
26. Rice, M. J.: 1979, Phys. Lett. 71A, p. 152.
27. Chien, S. N., Heeger, A. J., Kiss, Z., MacDiarmid, A. G., Gau, S. C., and Peebles, D. L.: Appl. Phys. Lett. (to be published)
28. Ooshika, Y.: 1957, J. Phys. Soc. Japan 12, pp. 1238, 1246.
29. Fincher, C. R., Jr., Ozaki, M., Tanaka, M., Peebles, D. L., Lauchlan, L., Heeger, A. J. and MacDiarmid, A. G.: Phys. Rev. B (Aug. 15, 1979).

30. Ito, T., Shirakawa, H., and Ikeda, S.: 1975, J. Polym. Sci., Chem. Ed. 13, p. 1943.
31. Fincher, C. R., Jr., Ozaki, M., Heeger, A. J., and MacDiarmid, A. G.: 1979, Phys. Rev. B 19, p. 4140.
32. Bychkov, Y. A., Gorkov, L. P., and Dzyaloshinskii, I. E.: 1966, Sov. Phys. JETP 23, p. 489.
33. Tani, T., Gill, W. D., Clarke, T. C., and Street, G. B.: Preprint, IBM Symposium on Conducting Polymers, March 29, 30, 1979.
34. Nigrey, P. J., MacDiarmid, A. G., and Heeger, A. J.: (in press, 1979), Chem. Commun. This paper discusses electrochemical doping techniques.
35. Park, Y. W., Denenstein, A., Chiang, C. K., Heeger, A. J., and MacDiarmid, A. G.: 1979, Sol. State Commun. 29, p. 747.
36. Kwak, J. F., Clarke, T. C., Greene, R. L., and Street, G. B.: 1978, Bull. Am. Phys. Soc. 23, p. 56.
37. Heikes, R.: "Buhl International Conference on Materials", Ed. by E. R. Shatz (Gordon and Breach, New York, 1974).
38. Chaikin, P. M. and Beni, G.: 1976, Phys. Rev. B 13, p. 647.
39. Harada, T., Shirakawa, H., and Ikeda, S.: Chem. Lett. (to be published; Street, G. B. (private commun.).
40. Salaneck, W. R., Thomas, H. R., Duke, C. B., Paton, A., Plummer, E. W., Heeger, A. J., and MacDiarmid, A. G.: J. Chem. Phys. (in press).
41. Fincher, C. R., Jr., Ph.D. Thesis, U. of Pennsylvania (1979) (unpublished).
42. Tanaka, M., Fincher, C. R., Jr., Heeger, A. J., Druy, M. A., and MacDiarmid, A. G.: 1979, Bull. Am. Phys. Soc. 24, p. 327.
43. Shirakawa, H. and Ikeda, S.: 1971, Polym. J. 2, p. 231; Shirakawa, H., Ito, T., and Ikeda, S.: 1973, Polym. J. 4, p. 460; Ito, T., Shirakawa, H., and Ikeda, S.: 1974, J. Polym. Sci. Polym. Chem. Ed. 12, p. 11; Ito, T., Shirakawa, H., and Ikeda, S.: 1975, J. Polym. Sci. Polym. Chem. Ed. 13, p. 1943.
44. Shirakawa, H. (private communication).
45. Seeger, K., Gill, W. D., Clarke, T. C., and Street, G. B.: 1978, Solid State Commun. 28, p. 873.
46. Mott, N. F.: 1972, Advances in Physics 21, p. 785.
47. See for example, Ziman, J. M., "Principles of the Theory of Solids", (Cambridge Univ. Press, 1972) pp. 168-170.
48. Rice, M. J. and Timonen, J. (preprint)
49. Schrieffer, J. R., (private communication).
50. Horovitz, B., (private communication).
51. Peebles, D. L., Tanaka, M., Heeger, A. J., and MacDiarmid, A. G., (to be published).
52. Baughman, R. H., Ivory, D. M., Miller, G. G., Shacklette, L. W., and Chance, R. R.: Preprint, IBM Symposium on Conducting Polymers March 29-30, 1979; Shacklette, L. W., Chance, R. R., Ivory, D. M., Miller, G. G., and Baughman, R. H., "Synthetic Metals" (in press).

53. Kanezawa, K. K., Diaz, A. F., Gardini, G. P., Gill, W. D., Kwak, J. F., and Street, G. B.: 1979, Bull. Am. Phys. Soc. 24, p. 326; IBM Symposium on Conducting Polymers, March 29-30, 1979.
54. Wnek, G. E., Chien, J. C. W., Karasz, F. E., Druy, M. A., Park, Y. W., MacDiarmid, A. G., and Heeger, A. J., Polymer Lett. (in press).
55. Shirakawa, H. and Ikeda, S., IBM Symposium on Conducting Polymers, March 29-30, 1979 and ACS/AJS Chemical Congress, Honolulu, April 1-6, 1979.

TECHNICAL REPORT DISTRIBUTION LIST, GEN

	No. Copies
Office of Naval Research Attn: Code 472 800 North Quincy Street Arlington, Virginia 22217	2
ONR Branch Office Attn: Dr. George Sandoz 536 S. Clark Street Chicago, Illinois 60605	1
ONR Branch Office Attn: Scientific Dept. 715 Broadway New York, New York 10003	1
ONR Branch Office 1030 East Green Street Pasadena, California 91106	1
ONR Branch Office Attn: Dr. L. H. Peebles Building 114, Section D 666 Summer Street Boston, Massachusetts 02210	1
Director, Naval Research Laboratory Attn: Code 5100 Washington, D.C. 20390	1
The Assistant Secretary of the Navy (R,E&S) Department of the Navy Room 4E736, Pentagon Washington, D.C. 20350	1
Commander, Naval Air Systems Command Attn: Code 310C (H. Rosenwasser) Department of the Navy Washington, D.C. 20360	1
Defense Documentation Center Building 5, Cameron Station Alexandria, Virginia 22314	12
Dr. Fred Saalfeld Chemistry Division Naval Research Laboratory Washington, D.C. 20375	1
U.S. Army Research Office Attn: CRD-AA-IP P.O. Box 1211 Research Triangle Park, N.C. [illegible]	
Naval Ocean Systems Center Attn: Mr. Joe McCartney San Diego, California 92152	
Naval Weapons Center Attn: Dr. A. B. Amster, Chemistry Division China Lake, California 93555	
Naval Civil Engineering Laboratory Attn: Dr. R. W. Drisko Port Hueneme, California 93401	
Department of Physics & Chemistry Naval Postgraduate School Monterey, California 93940	
Dr. A. L. Slafkosky Scientific Advisor Commandant of the Marine Corps (Code RD-1) Washington, D.C. 20380	
Office of Naval Research Attn: Dr. Richard S. Miller 800 N. Quincy Street Arlington, Virginia 22217	
Naval Ship Research and Development Center Attn: Dr. G. Bosmajian, Applied Chemistry Division Annapolis, Maryland 21401	
Naval Ocean Systems Center Attn: Dr. S. Yamamoto, Marine Sciences Division San Diego, California 91232	
Mr. John Boyle Materials Branch Naval Ship Engineering Center Philadelphia, Pennsylvania 19112	

TECHNICAL REPORT DISTRIBUTION LIST, 356B

	No. Copies
Dr. T. C. Williams Union Carbide Corporation Chemical and Plastics Tarrytown Technical Center Tarrytown, New York	1
Dr. R. Soulen Contract Research Department Pennwalt Corporation 900 First Avenue King of Prussia, Pennsylvania 19406	1
Dr. A. G. MacDiarmid University of Pennsylvania Department of Chemistry Philadelphia, Pennsylvania 19174	1
Dr. C. Pittman University of Alabama Department of Chemistry University, Alabama 35486	1
Dr. H. Allcock Pennsylvania State University Department of Chemistry University Park, Pennsylvania 16802	1
Dr. M. Kenney Case-Western University Department of Chemistry Cleveland, Ohio 44106	1
Dr. R. Lenz University of Massachusetts Department of Chemistry Amherst, Massachusetts 01002	1
Dr. M. David Curtis University of Michigan Department of Chemistry Ann Arbor, Michigan 48105	1
Dr. M. Good Division of Engineering Research Louisiana State University Baton Rouge, Louisiana 70803	1
Douglas Aircraft Company 3855 Lakewood Boulevard Long Beach, California 90846 Attn: Technical Library C1 290/36-84 AUTO-Sutton	1
NASA-Lewis Research Center 21000 Brookpark Road Cleveland, Ohio 44135 Attn: Dr. T. T. Serafini, MS 49-1	1
Dr. J. Griffith Naval Research Laboratory Chemistry Section, Code 6120 Washington, D.C. 20375	1
Dr. G. Goodman Globe-Union Incorporated 5757 North Green Bay Avenue Milwaukee, Wisconsin 53201	1
Dr. E. Fischer, Code 2853 Naval Ship Research and Development Center Annapolis Division Annapolis, Maryland 21402	1
Dr. Martin H. Kaufman, Head Materials Research Branch (Code 4542) Naval Weapons Center China Lake, California 93555	1
Dr. J. Magill University of Pittsburg Metallurgical and Materials Engineering Pittsburg, Pennsylvania 22230	1
Dr. C. Allen University of Vermont Department of Chemistry Burlington, Vermont 05401	1
Dr. D. Bergbreiter Texas A&M University Department of Chemistry College Station, Texas 77843	1

TECHNICAL REPORT DISTRIBUTION LIST, 356B

	No. Copies
Professor R. Drago Department of Chemistry University of Illinois Urbana, Illinois 61801	1
Dr. F. Brinkman Chemical Stability & Corrosion Division Department of Commerce National Bureau of Standards Washington, D.C. 20234	1
Professor H. A. Titus Department of Electrical Engineering Naval Postgraduate School Monterey, California 93940	1
COL B. E. Clark, Code 100M Office of Naval Research 800 N. Quincy Street Arlington, Virginia 22217	1
Professor T. Katz Department of Chemistry Columbia University New York, New York 10027	1
Dr. Frank Karasz Department of Polymer Science and Engineering University of Massachusetts Amherst, Massachusetts 01003	1
Dr. James Chien Department of Polymer Science and Engineering University of Massachusetts Amherst, Massachusetts 01003	1
Professor A. J. Heeger Director Laboratory for Research on Structure of Matter 33rd and Walnut Streets/K1 University of Pennsylvania Philadelphia, Pennsylvania 19104	1
Dr. Richard A. Reynolds Deputy Director Defense Sciences Office DARPA 1400 Wilson Blvd. Arlington, Virginia 22209	1
Dr. Rudolph J. Marcus Office of Naval Research Scientific Liaison Group American Embassy APO San Francisco 96503	1
Mr. James Kelley DTNSRDC Code 2803 Annapolis, Maryland 21402	1


DATE
ILMED
-8